九州大学学術情報リポジトリ
Kyushu University Institutional Repository

Amplifier-assisted cavity ring-down spectroscopy using optical waveguide

李, 雯穎

https://hdl.handle.net/2324/4110524

出版情報：Kyushu University, 2020, 博士（工学）, 課程博士
バージョン：
権利関係：

Amplifier-assisted cavity ring-down spectroscopy using optical waveguide

Interdisciplinary Graduate school of Engineering Science,

Kyushu University

Hamamoto Laboratory

Wenying Li

Table of contents

Abstract

Population aging problem has become one of the significant social problem. Because of this problem, the demand of daily and easy health-check system for elder people is considered to be important. Especially home-based health monitor is desired. Breath sensing is available for the daily and easy health check because exhaled breath contains a lot kinds of disease markers. People only need breathing-out toward the sensor. The density of each disease marker in breath is analyzed at the time.

For home-use, breath sensor based on infrared absorption spectroscopy has the possibility to sense several kinds of gases at the same time. This is because each gas has its own eigen absorption peak in wavelength. For sensing ppm-order gas component in breath by using infrared absorption, an extremely long optical sensing path of several km is needed for sufficient light absorption (typically 3 dB). To achieve the effectively long length sensing path (corresponding km order) within a cavity, CRDS (cavity ring-down spectroscopy) has been proposed. One issue of the CRDS system as home-use sensor is its large size.

We have proposed breath sensor utilizing optical waveguide as the optical path for infrared absorption based on CRDS. This is because waveguide is capable for integrating several meter optical paths in a compact

area (1 cm^2). One problem is the waveguide propagation loss. Huge amount of loss decreases the sensing light intensity. As most of the sensing light intensity is reduced due to the propagation loss, ppm-order breath sensing becomes hard to be realized. As a solution, we have proposed amplifier-assisted CRDS to compensate the propagation loss. For hand-held breath sensor, SOA (semiconductor optical amplifier) is a candidate due to its capability of integration. To verify the effectiveness of the amplifier-assisted CRDS, we use an EDFA (Erbium-doped fiber amplifier) instead of the SOA inside CRDS system in this work. When EDFA is at a high pumping condition, ASE (amplified spontaneous emission) loops inside CRDS system and be amplified in the EDFA. Then, it starts self-lasing at a wavelength different from sensing light. Once self-lasing happens, sensing light looses the gain from EDFA. This is because most of the gain is attributed to lasing wavelength. We have proposed polarization direction control scheme to suspend self-lasing by weakening the coherency condition. The coherency is a fundamental requirement of making oscillation in cavity (namely, ring-cavity here) in general. The result showed that the self-lasing intensity was suspended, and the gain was improved to 24 dB from 14 dB at the sensing light wavelength.

Whereas the self-lasing issue has been improved, there is still an important issue in the amplifier-assisted CRDS system. The amplifier noise

which exists at sensing light wavelength is hardly eliminated. In ppm-order gas sensing, the amplifier noise loops inside the system with sensing light for more than 1,000 times. The significant accumulated noise intensity may surpass the sensing light intensity and prevent ppm-order breath sensing. Hence, the accumulated noise intensity influences the sensing ability of amplifier-assisted CRDS system directly. In this work, to evaluate the lowest gas sensing concentration of amplifier-assisted waveguide CRDS, we calculated the accumulated amplifier noise intensity at ppm-order gas sensing condition. Then we estimated the necessary injection light intensity for ppm-order gas sensing under the influence of the amplifier noise. The estimated results showed several kinds of ppm-order gases (CO_2, CH_4, NH_3, and CH_3COCH_3) are sensing-available by using the injection light intensity below 10 mW when the criteria level is set as 0.9. Meanwhile, the actual 3% CO_2 sensing was also demonstrated experimentally to confirm the effectiveness of this proposal shown in this thesis.

Chapter 1

Introduction

1.1 Research background

Population aging becomes one of the most significant social problems of the twenty-first century. Figure 1.1 shows the young and elderly global population in percentage. As shown in this figure, up to 2020, the number of people over 65 crosses over under age 5. Due to decrease of birth-rate and remarkable increases in life expectancy, population aging continues, and even accelerates [1].

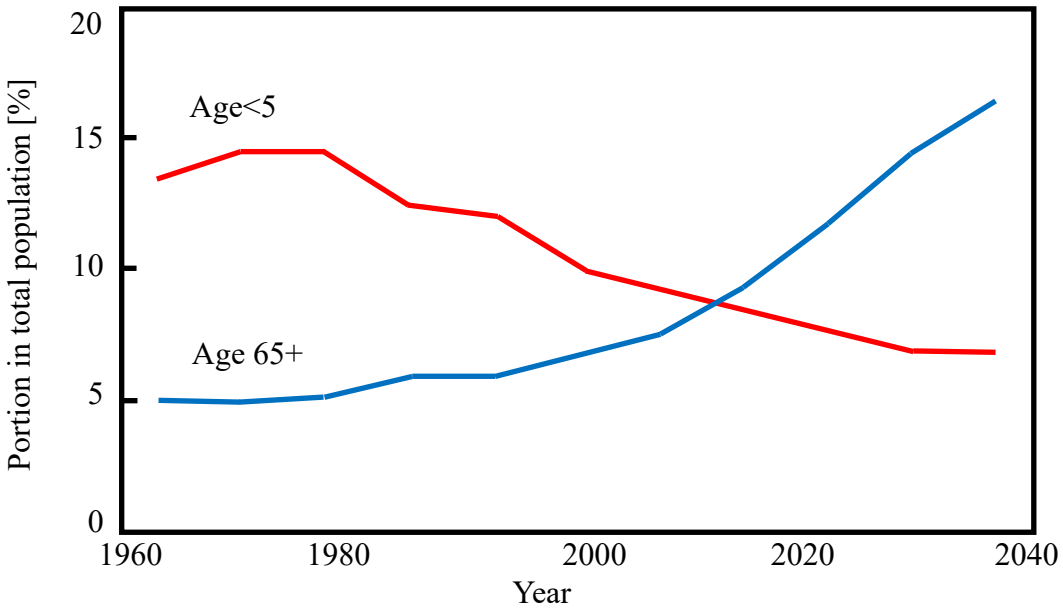

Fig. 1.1 Young and elderly global population in percentage. The number of people over 65 crosses over under age 5 up to 2020. Population aging problem continues, and even accelerates.

As the elderly global population increasing, the health care for the elderly becomes a serious challenge [2]. This is because the medical resources and the manpower of health care for the elderly may be in short supply [3].

The health check in hospital is already mature technology. radioactive rays (e.g. X-rays, computed tomography), ultrasonic (e.g. type-B ultrasonic, color ultrasound examination), and nuclear magnetic resonance imaging [4-7] are the typical examples. These health check machine; however; must be operated by professionals. When the number of the elderly is far beyond the control of the professionals, the health care of the elderly is not guaranteed. Therefore, the demand of home-based health monitor with easy operation for daily health care is increasing [8].

The home-health care technology has been widely researched [9-12]. We summarized these researches in Tab. 1.1. As shown in this table, these researches are based on urine test or blood test. By measuring the urine and the blood of people, a lot of body health parameters are detectable. Besides these researches, the home-health-monitoring products also been produced [13-15]. These products are summarized in Tab. 1.2.

The health monitors shown in Tab. 1.1 and Tab. 1.2; however; only contains the information of one kind of disease. Meanwhile, some of these products are invasive (such as blood test), troublesome operation (such as urine test), need professional support to analyze the testing result and identify

a disease and time cost (such as electrocardiogram).

Tab. 1.1 Researches about home-based health monitor. The urine test and the blood test have troublesome operation. The troublesome operation increases the difficulty to sense diseases.

Year	Nation	Institute	Detection method	Detection disease	Size	Ref.
2014	The Netherlands	Radboud Univ.	Urine test	Kidney disease	Smart phone based	[9]
2006	Japan	Kanazawa Univ.	Urine test	Urine glucose level		[10]
2019	America	Johns Hopkins Univ. School of Medicine	Urine test	Prenatal care for woman	Smart phone based	[11]
2019	China	Hangzhou Dianzi Univ.	Blood test	blood lipid data acquisition for cardiovascular disease	Smart phone based	[12]

Tab. 1.2 Home-based health monitor products. These products are either invasive or need professional support to analyze the testing result.

Nation	Company	Detection item	Size	Price	Ref.
Japan	Omron	Blood pressure	L×W×H 191×120×85 mm	20,000	[13]
Japan	Omron	Blood glucose	L×W×H 43.2×74.7×16.3mm	15,000 yen	[14]
America	Scripps Translational Science Institute	Continuous Electrocardiogram (ECG)			[15]

A health check method for several kinds of diseases detection at the same time is desired. Human exhaled breath contains a lot kinds of disease markers [16, 17]. Breath test has the potential for several diseases detection. Breath test is noninvasive. People only need breathing-out toward the breath sensor. The density of each disease marker in breath is analyzed at the time.

Exhaled breath contains several different volatile-gases. The breath component portion in exhaled human-breath are shown in Fig. 1.2.

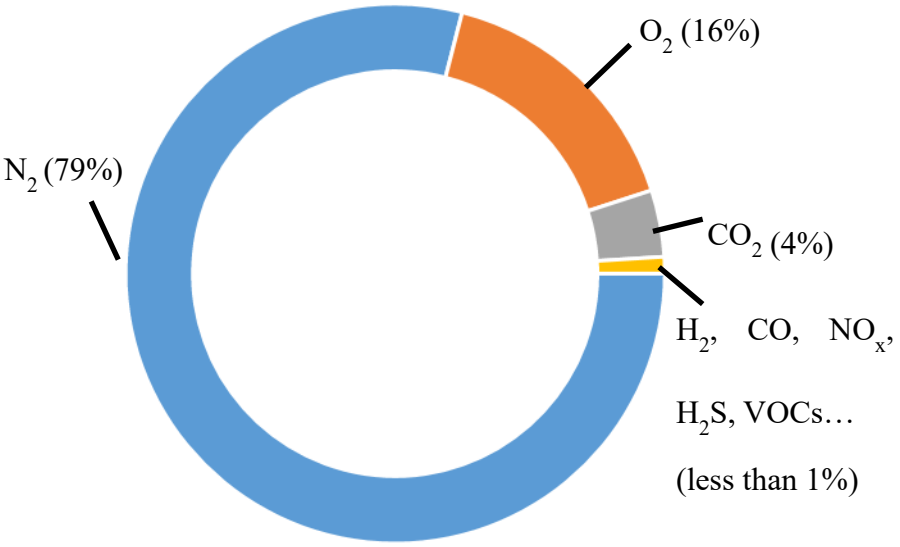

Fig. 1.2 Breath component portion in exhaled breath. The less than 1% part that is shown in yellow includes NO_x and VOCs. The NO_x and VOCs are important volatile-gases as diseases markers.

The composition of exhaled breath (excluding saturated water vapor) is about 80% nitrogen (N_2), 16% oxygen (O_2), and 4% carbon dioxide (CO_2). The rest part is less than 1%; however; the rest includes important volatile-gases as diseases markers. It is consisted of hydrogen (H_2), carbon monoxide

(CO), nitrogen oxide (NO_x), hydrogen sulfide (H_2S), and volatile organic compounds (VOCs) [18]. NO_x and VOCs are disease-markers that are used for hearth-monitoring [19-21]. The concentration of these gases in exhaled breath indicate the potential of some diseases. The breath contents and their related diseases are summarized in Tab. 1.4.

Tab. 1.4 Breath contents and related diseases. The breath contents have potential for sensing many kinds of diseases.

Breath contents	Concentration	Related disease	Ref.
Methane (CH_4)	2-10 ppm	Intestine disease	[22-24]
Carbon monoxide (CO)	1-10 ppm	Lung disease, asthmatic	[25, 26]
	3.3-4.7 ppm	Type 1 diabetes	[27]
	4.6-5.4 ppm	Type 2 diabetes	
Breath contents	Concentration	Related disease	Ref.
Ammonia (NH_3)	0.5-5 ppm	Liver disease	[28]
Nitric oxide (NO)	10-2000 ppb	Asthma, allergic rhinitis	[29]
Acetone (CH_3COCH_3)	1.7-3.7 ppm	Diabetes	[30, 31]
	0.1-2 ppm	Body fat	[32]
Ethane (C_2H_6)	0-10 ppm	Vitamin E status, lipid peroxidation	[33-35]
Isoprene (C_5H_8)	50-200 ppb	Hyper-cholesterol	[36]
Pentane (C_5H_{12})	0-10 ppb	Lipid peroxidation	[37]
Hydrogen peroxide (H_2O_2)		Oxidative stress, lung disease	[38-41]
		Lipid peroxidation	[42]

1.2 Breath sensing: State of the arts

Sensing exhaled breath is one of the easy ways of health check. Up to now, several commercial products of breath sensor have been developed [43-46]. They are summarized in Tab. 1.5. As shown in this table, the prices of these products are all very expensive. The sizes of these sensors are not compact enough for home-use.

Tab. 1.5 Gas sensing products. The gas sensing products listed in this table are too expensive for normal family purchase. The size of these products are not small enough for family use.

Nation	Company	Detection method	Detection item	Size [mm]	Price	Ref.
Japan	Otuska	Infrared absorption	Helicobacter pylori	220×361 ×272	0.96 Million JPY	[43]
Japan	Anima	Infrared absorption	Respiratory metabolism for calories burned calculation	Sensor part 134×208 ×77	4.98 million JPY	[44]
Japan	Horiba	Infrared absorption	CO, CO_2 CH_4, N2O NO, SO_2 NH_3	430×550 ×221	2.5 million JPY ~	[45]
America	Tiger Optics	Infrared absorption	CH_4, N_2O CO, CO_2 NH_3, H_2S	222×483 ×599	Few million JPY ~	[46]

Besides the commercial products that are introduced above, there are many researches about the gas sensor [47-57]. Based on the different sensing principle of the gas sensors, the sensors are divided into direct sensing type and indirect sensing type. We summarized the researches of the gas sensors

in Tab. 1.6 (indirect sensing type) and Tab. 1.7 (direct sensing type).

Tab. 1.6 Indirect sensing type **s**ensors summary. The Indirect sensing type **s**ensors have high sensitivity. The sensing target gas must be decided.

Year	Nation	Institute	Sensing principle	Size [mm]	Sensing time	Detectable gas	Ref.
2010	Japan	Fujitsu	Frequency change	25×25×9	Real-time		[47]
2017	Japan	Fujitsu	Resistance change	1×1 ×0.001	10 s	NH_3	[48]
2013	Japan	AIST	Resistance change	5×5×1	10 mins	H_2	[49]
2018	Japan	Hitachi	Resistance change	30×40×5	<3 s	Alcohol	[50]
2013	Japan	NIMS	Resistance change	0.5×0.5 ×0.003	1.3 s		[51, 52]
2016	Japan	Panasonic	Transmittance change	5×5 ×0.0005		NO	[53]
2008	America	West Texas *A&M* Univ. & Mississippi State Univ.	Infrared spectroscopy			NH_3	[54]
2018	Sweden	Royal Institute of Tech.	Resistance change	10×10×1	21 s	H_2S	[55]
2016	Germany	Heinrich Heine Univ. Düsseldorf	Resistance change	3.5×3.5 ×0.13		CO/H_2	[56]
2014	Spain	Univ. of Navarra	Refractive index change				[57]

Tab. 1.7 Direct sensing type sensors summary. Direct sensing type sensors are possible for sensing many kinds of gases. It is available for daily use.

Year	Nation	Institute	Sensing principle	Size [mm]	Sensing time	Detectable gas	Ref.
2016	Japan	Tohoku Univ.	UV spectroscopy	600 ×600	Realtime	All kinds	[58]
2015	Japan	Toshiba	Infrared spectroscopy		Realtime	All kinds	[59]
2017	America	IBM	Infrared spectroscopy	2.5×5	Realtime	All kinds	[60]
2006	America	Ekips Technology	Infrared spectroscopy	3.6 $\times 10^5$	Realtime	NO	[61]
2014	America	Physical Sciences Inc.	Infrared spectroscopy	500 ×500 ×250	Realtime	CH_4/CO_2	[62]
2005	Germany	Univ. Düsseldorf	Infrared spectroscopy	600 ×800	Realtime	All kinds	[63, 64]

Indirect sensing relies on the reaction between gas and some materials, through measuring the generated change of resistance, refractive index, frequency, or the transmittance to estimate gas concentration. In [48] for instance, the Cu ions in material CuBr reacts with the ammonia gas (NH_3). The reaction forms coordination complex. The coordination complex traps the Cu ions, causing the carrier concentration decrease. The resistance of the CuBr is changed. The concentration of NH3 is estimated by detecting the voltage change of the CuBr.

The indirect type sensors have high sensing sensitivity. Usually, the indirect type sensors are suitable for sensing gas concentration burst change. Indirect type sensors utilizing in daily health care may have drift problem.

The sensing part's surface may get dirty or damage after several times using. The drift problem may result in low sensing accuracy. For instance, in [48] that mentioned above, once the CuBr reacted with NH_3, it is not available for NH_3 sensing anymore. Therefore, this kind of gas sensors are not suitable for daily use. Moreover, the sensing target gas must be decided. Breath sensor with only one kind of gas sensing contains little health information.

Direct sensing estimates the change of gas physical quantities, such as mass-sensitive, chromatography, and infrared absorption spectroscopy [65-67]. The direct sensing type sensors have gas selectivity. The sensing is real-time as shown in Tab. 1.7.

For home-use, breath sensor is desired to realize several diseases detection at one time. Among the sensors that are summarized in Tab. 1.6, and Tab. 1.6, gas sensors based on infrared absorption spectroscopy has the possibility to sense several gases simultaneously [68-70]. This is because each gas has its own eigen absorption peak in wavelength [71]. Table 1.8 summarize breath contents, absorption wavelength and their absorption cross-section [72, 73]. Gas absorption abilities are decided by absorption cross-section. A large absorption cross-section indicates a strong absorption ability.

Tab. 1.8 Breath contents and their absorption wavelength and absorption cross-section. Different gas has its eigen absorption wavelength. The absorption abilities are different at different absorption wavelength.

Breath content	Absorption wavelength [μm]	Absorption cross-section [cm^2]
Methane (CH_4)	1.65	1.6×10^{-20}
	2.35	5.2×10^{-21}
	3.25&3.26	2.1×10^{-19}
Carbon monoxide (CO)	1.57	2.2×10^{-23}
	2.33	1.2×10^{-20}
	4.60	4.5×10^{-19}
Ammonia (NH_3)	1.51	2.5×10^{-20}
	3.00	1.2×10^{-19}
	6.15	3.1×10^{-19}
Nitric oxide (NO)	1.79	5.5×10^{-23}
	2.66	1.1×10^{-21}
Acetone (CH_3COCH_3)	1.56	1.2×10^{-24}
	1.68&1.69	3.6×10^{-22}
	2.12	4.2×10^{-22}
Carbon dioxide (CO_2)	1.57	7.7×10^{-23}
Ethane (C_2H_6)	1.7	1.5×10^{-20}
	3.35	1.7×10^{-18}

Different gas has its eigen absorption wavelength [74]. Several kinds of gases are detectable simultaneously by using infrared absorption spectroscopy with varying wavelength within a certain absorption wavelength band. The sensing principle configuration of infrared absorption spectroscopy is shown in Fig. 1.3.

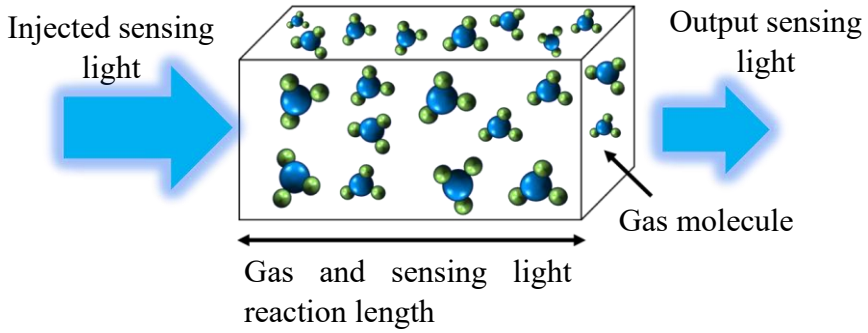

Fig. 1.3 Infrared absorption spectroscopy configuration. Sensing light is absorbed by gas. The gas concentration is estimated by the injected and output sensing light intensity.

As shown in Fig. 1.3, the injected sensing light propagates through the gas area. The light intensity decreases due to gas absorption when the wavelength is exactly adjusted to the eigen absorption one of the gas-molecule. The gas concentration is estimated by measuring the difference between injected and output sensing light intensity. As mentioned in Tab. 1.4, the gas concentration in exhaled breath are all at ppm-order. For sensing ppm-order breath component by using infrared absorption spectroscopy, an extremely long optical sensing path (shown in Fig. 1.3: gas and sensing light reaction length) of several km is needed for sufficient light absorption (typically 3 dB). To achieve the effective long-length sensing path (corresponding km order), CRDS (cavity ring-down spectroscopy) [64] has been proposed. The configuration of the CRDS system is shown in Fig. 1.4. The cavity has high-reflective mirrors on both facets. The effective km length sensing path is realized by multiple reflections at the cavity-mirrors. In case when the mirror reflective index is set to be higher than 99.9%, 1,000

times reflection is achieved. If we use a meter-long cavity for instance, the effective length may exceed km order. One issue of the CRDS system as home-use sensor is its large cavity size. To realize hand-held size gas sensor, in this research, we use optical waveguide as the sensing path. This is because optical waveguide realizes several meter optical paths integrating in a compact area (1cm^2) [75-77].

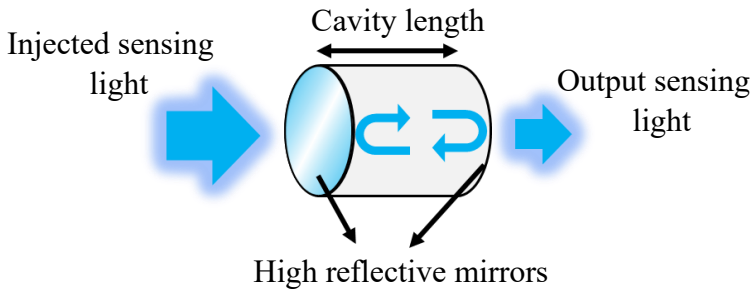

Fig. 1.4 CRDS system configuration. The cavity has high reflective mirrors on both facets. The effective km-order sensing path is achieved by reflecting the sensing light inside the cavity for thousands times.

1.3 Amplifier-assisted waveguide CRDS toward compact breath sensing

To realize hand-held size breath sensor for home-use health check, we proposed optical waveguide as the sensing path. In this section, we firstly introduce the optical waveguide for sensing path in section 1.3.1. Then, we introduce the configuration of the integrated optical sensing circuit and the experimental system in session 1.3.2. Next, we introduce the issues and the solutions of the optical sensing circuit in session 1.3.3.

1.3.1 Optical waveguide for sensing path

Optical waveguide is proposed as the sensing path to realize hand-held gas sensor. One requirement of sensing waveguide is that the gas need to touch the sensing light for gas absorption. For example, the buried type waveguide [79] shown in Fig. 1.5 is not suitable for gas sensing. When the sensing light propagates in the core of the buried waveguide, the gas is unable to touch the sensing light. Thus, the gas absorption does not happen.

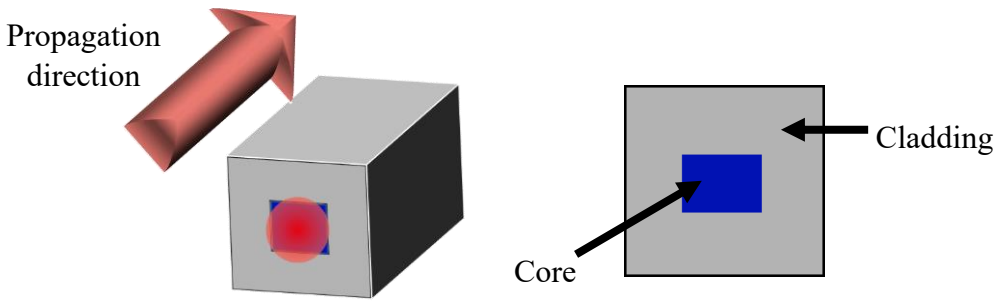

Fig. 1.5 Buried waveguide structure. The sensing light propagates in the core in the middle of the waveguide. Gas does not touch the sensing light. The gas absorption does not happen. Therefore, the buried type waveguide is not suitable for gas sensing.

As shown in Fig. 1.6, there are four types of waveguide structures [75-77, 80-87] that are capable for gas sensing. When lights propagate in these four types waveguide, a certain portion of light profiles out of the waveguide (shown in the left-hand side of Fig. 1.6). This part of sensing light is used for gas absorption.

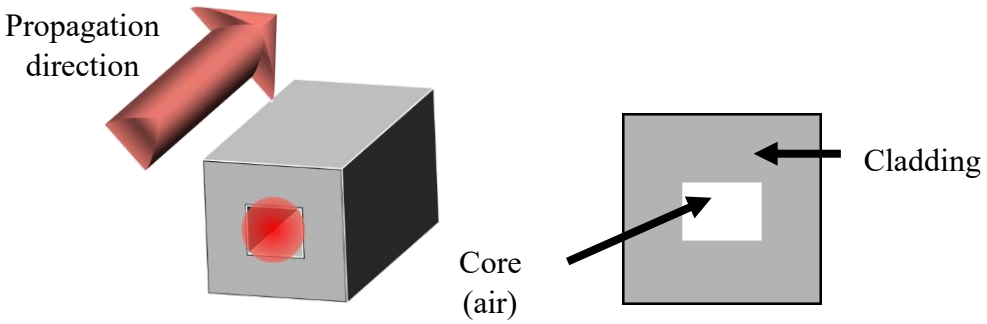

(a) Hollow type waveguide structure

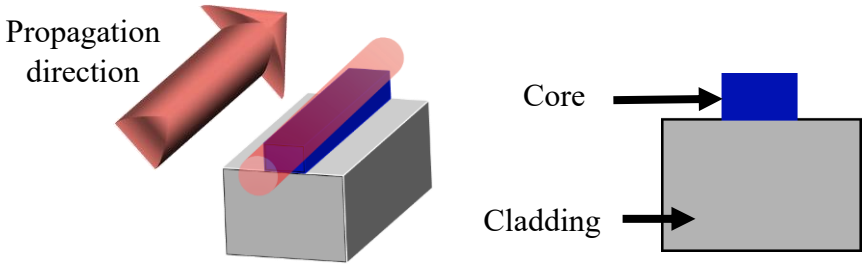

(b) Strip type waveguide structure

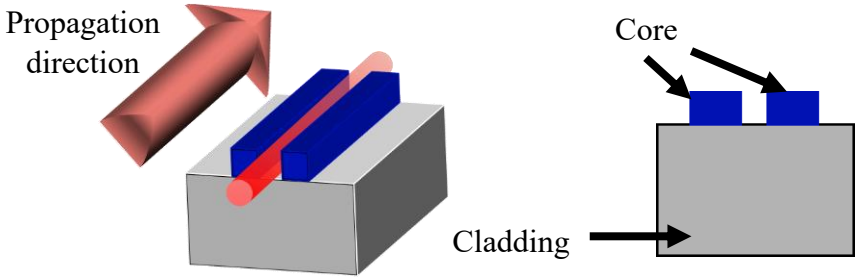

(c) Slot type waveguide structure

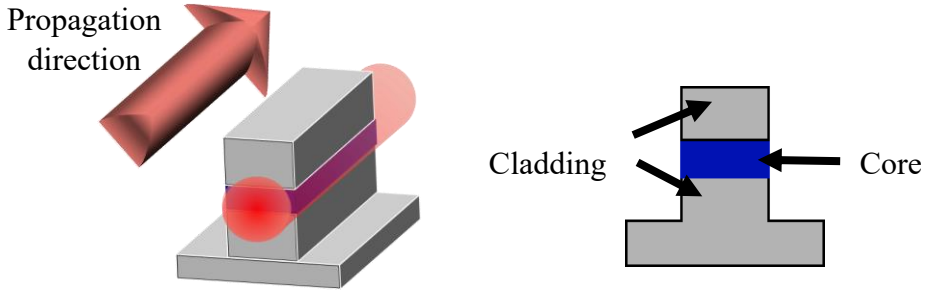

(d) High-mesa type waveguide structure

Fig. 1.6 Four types of waveguide structures. These four types of waveguide are all available for gas sensing. This is because the outside gas touches the sensing light and absorbs the light intensity.

To compare these four types waveguide in details, the characteristics of these four types waveguide [87-90] are summarized in Tab. 1.9. As shown in this table, it is clear that strip type and high-mesa type waveguide are more suitable for gas sensing than the other two types.

Tab. 1.9 Characteristics of four types waveguide. The strip type and high-mesa waveguide are suitable for gas sensing than the other two types waveguide.

Waveguide type	Easy for touching gas	Easy for fabrication	Light easy for coming out of waveguide	Propagation loss
Hollow type	☹	☹	☺ ☺	0.02 dB/cm
Strip type	☺ ☺	☺ ☺	☺	
Slot type	☺	☹	☺ ☺	12 dB/cm
High-mesa type	☺ ☺	☺ ☺	☺	0.02 dB/cm

The strip type waveguide; however; has drift problem. After long time using, the waveguide core surface may be covered with dust. The dust may cause a large scattering loss. The large scattering loss consumes the sensing light intensity and results in flow sensing accuracy. While in the case of high-mesa waveguide, the sensing light comes out from the sidewall of the waveguide. Sidewall is less in dust-stacking compared to the strip type waveguide. Hence, high-mesa waveguide is a good choice for gas sensing.

There are two parameters to evaluate the waveguide performance in gas sensing: the waveguide propagation loss α [dB/cm] and the portion of light

for gas absorption Γair [%]. The propagation loss decreases the sensing light intensity. As most of the sensing light intensity is reduced due to the propagation loss, the rest part of sensing light intensity is not sufficient to propagate in the waveguide for many times. The corresponding sensing path length is too short to sense ppm-order breath components. Therefore, waveguide propagation loss is desired as low as possible.

The light field distribution in the waveguide is shown in Fig. 1.7. The portion of light profile Γair is defined as:

$$\Gamma air = \frac{Light\ intensity\ profiling\ out\ from\ waveguide: (B+C)}{The\ total\ sensing\ light\ intensity: (A+B+C)} \times 100\% \qquad (1.1)$$

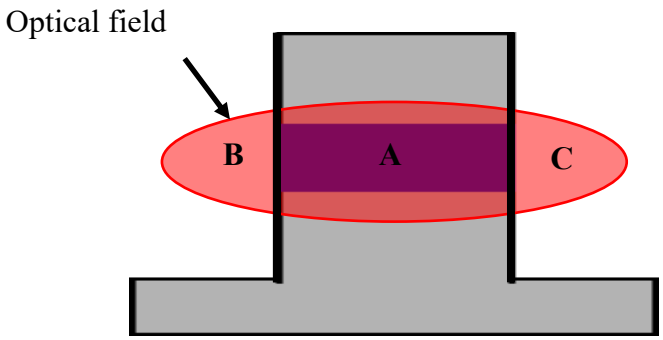

Fig. 1.7 Optical field distribution in waveguide. Part B and C are the light that profiles out of the waveguide for gas absorption.

A high Γair is expected. This is because higher Γair means more light intensity being used for gas absorption. α and Γair are dependent on the structure and the material of the high-mesa waveguide. Figure 1.8 shows two high-mesa waveguide structures with different materials. The waveguide

structure in Fig. 1.8 (a) is silica high-mesa waveguide [87]. The core is germanium-doped silica (Ge-doped SiO_2) and the clad is pure silica (SiO_2). The waveguide structure in Fig. 1.8 (b) is silicon high-mesa waveguide [91]. The core is silicon (Si) and the clad is silica (SiO_2). Figure 1.9 and Fig. 1.10 show the values of α and Γair as a function of waveguide width of silica and silicon high-mesa waveguide, respectively [87, 91].

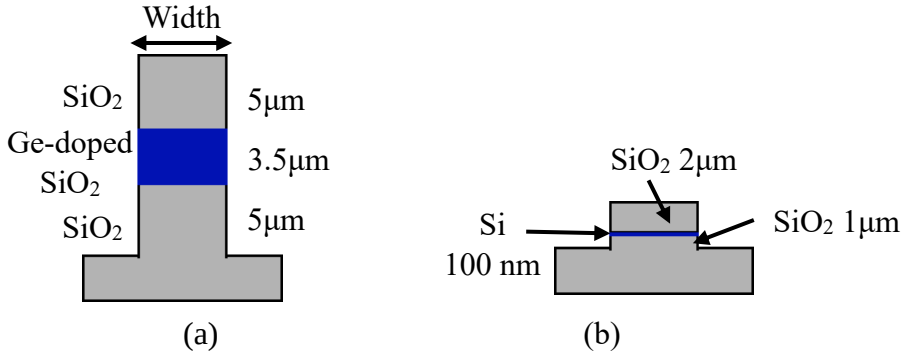

Fig. 1.8 High-mesa waveguide structures. (a) Silica high-mesa waveguide, and (b) silicon high-mesa waveguide [87, 91].

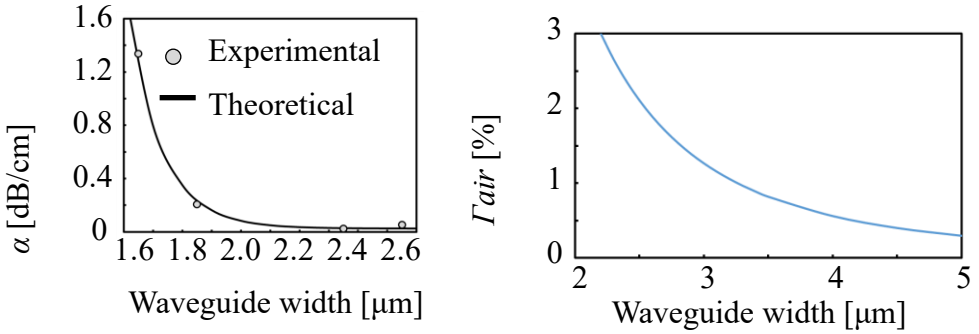

Fig. 1.9 Silica high-mesa waveguide α and Γair as a function of waveguide width [87, 91]. Silica high-mesa waveguide has a low α as to 0.02 dB/cm. The highest Γair is 3%.

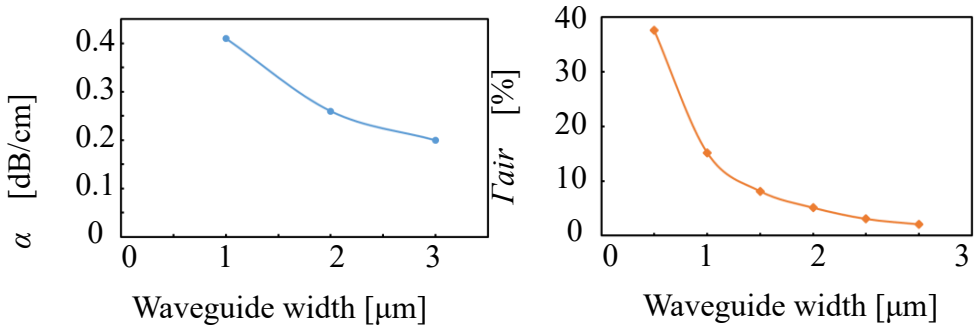

Fig. 1.10 Silicon high-mesa waveguide α and Γair as a function of waveguide width [87, 91]. Silicon high-mesa waveguide has a high Γair as to 37%. Meanwhile, its α is as large as 0.4 dB/cm.

As shown in Fig. 1.9, silica high-mesa waveguide reaches an extremely low propagation loss of 0.02 dB/cm. While the highest Γair is only 3%. In Fig. 1.10, silicon high-mesa waveguide gets the high Γair of 37%, while the propagation loss is as large as 0.4 dB/cm. To evaluate the sensing waveguide performance with α and Γair, an evaluation parameter FOM (figure of merits) [92] is defined as:

$$FOM = \frac{\Gamma air}{\alpha} \tag{1.2}$$

A high Γair and a low α (expected in sensing waveguide) make a high FOM. Therefore, FOM is used to evaluate the performance of the sensing waveguide. A high FOM value indicates a high sensing sensitivity of the waveguide. In the cases of silica high-mesa waveguide and silicon high-mesa waveguide that mentioned in Fig. 1.8, the FOM are estimated as 1.35 and 0.4, respectively. Apparently, silica high-mesa waveguide has a better performance than silicon high-mesa waveguide.

In this research, we use the structure of silica high-mesa waveguide for gas sensing. The propagation loss and the *Γair* are 0.02 dB/cm and 2.7%, respectively.

1.3.2 Amplifier-assisted waveguide CRDS configuration

The gas sensing in this research is based on infrared absorption spectroscopy utilizing CRDS system. Optical waveguide is used as the sensing path in CRDS system. A future version of the integrated optical sensing circuit configuration is shown in Fig. 1.11.

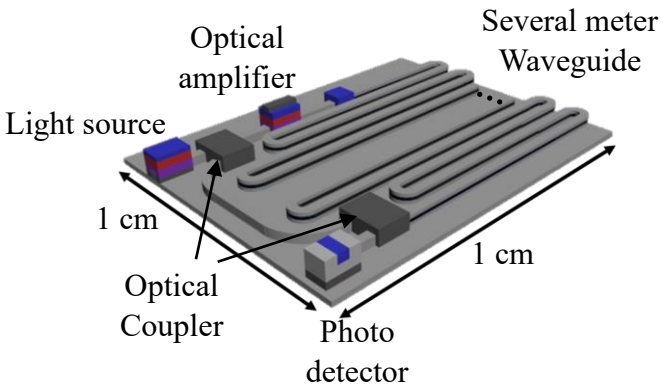

Fig. 1.11 Future version of the integrated optical sensing circuit configuration. Several meter sensing waveguide is integrating on a 1 cm × 1 cm size chip.

As shown in this figure, several-meter-long waveguide is integrated on the chip. The “cavity” in CRDS system is consisted of waveguide and two optical couplers. Sensing light coming out from light source is injected into the waveguide via an optical coupler. The sensing light is absorbed by gas

while propagating through the waveguide. When the sensing light propagates to the end port of the waveguide, a portion of light is guided to photo detector for detecting light intensity. The rest part of the sensing light is guided back to the input port of the waveguide for gas absorption via the optical couplers.

Because the sensing waveguide is several-meter-long, the sensing light propagating in waveguide for 1,000 times corresponds to a sensing path of km-order. As mentioned in section 1.2, km-order length sensing path is available for ppm-order breath contents detection. Therefore, this integrated optical sensing circuit has potential for breath sensing.

One problem is the waveguide propagation loss. Huge amount of loss decreases the sensing light intensity. As most of the sensing light intensity is reduced due to the propagation loss, ppm-order breath sensing becomes hard to be realized. As a solution, we have proposed amplifier-assisted CRDS system [64]. Figure 1.12 shows the configuration of the amplifier-assisted CRDS system. an optical amplifier is set in the waveguide CRDS system to compensate the propagation loss.

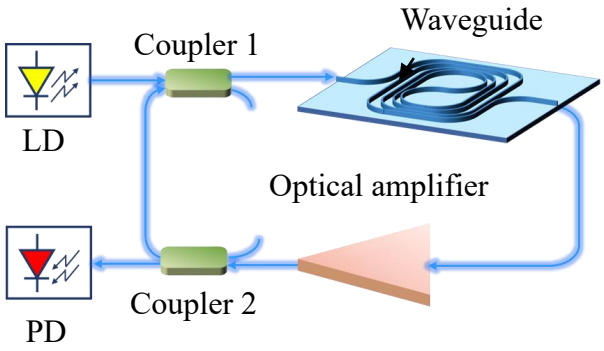

Fig. 1.12 Configuration of the amplifier-assisted waveguide CRDS. An optical amplifier is set inside the waveguide CRDS to compensate the propagation loss.

There are many kinds of optical amplifiers. Fig. 1.13 shows a "family tree" of the optical amplifiers [93].

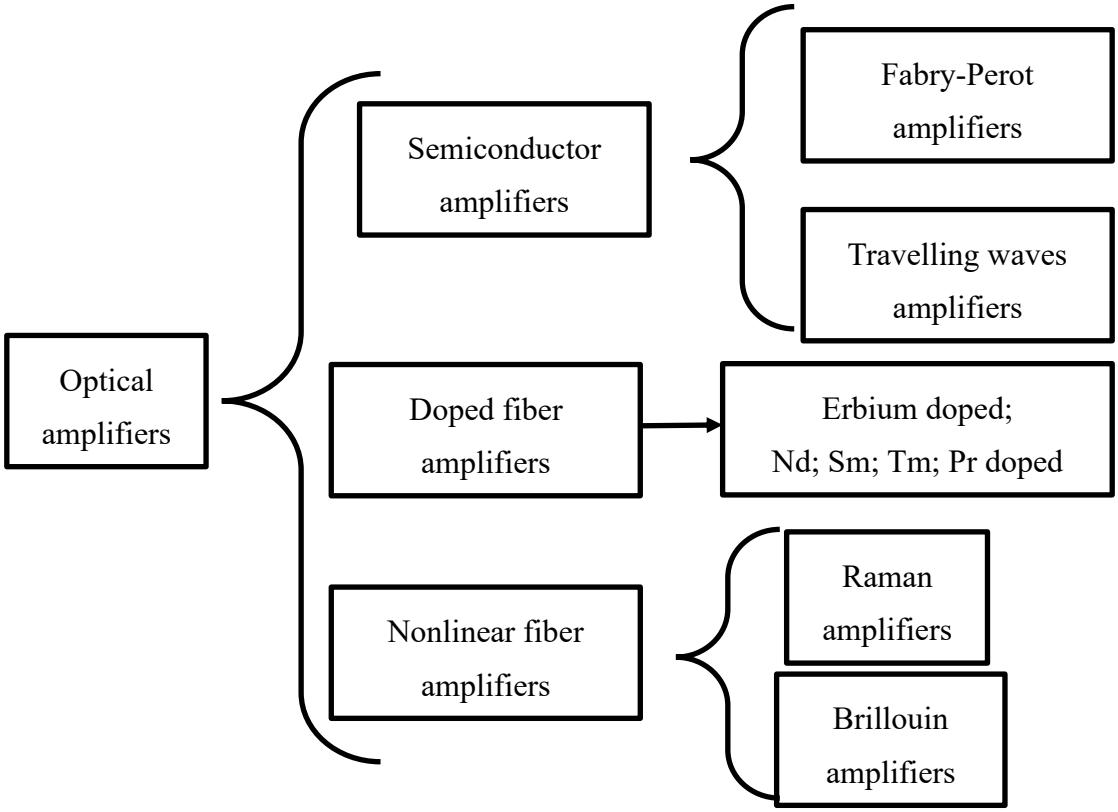

Fig. 1.13 "Family tree" of optical amplifiers [93]. There are many kinds of optical amplifier. These optical amplifiers have different amplification performance.

The proper optical amplifier is chosen according to the amplification requirement. The performance of the optical amplifiers that are mainly be used [93] are summarized in Tab. 1.10.

For integrated optical sensing circuit, SOA (semiconductor optical amplifier) is a candidate due to its capability of integration [94].

Tab. 1.10 Main features of different optical amplifiers [93]. Different type of optical amplifier has different amplification wavelength and gain. The amplifier size is also different.

	SOA F-P type	SOA T-W type	EDFA	Raman
Gain [dB]	30	20~30	30~45	20~45
Amplification wavelength [nm]	850 ~ 1600	850~ 1600	1525 ~ 1605	300 ~ 2000
Output power [dBm]	+10	-10 ~-5	+5~ +10	+30
Polarization sensitivity		Yes	No	No
Power supply	100~200mA (current)	20 mA (current)	20-200 mW	1-5 W
Size	μm order	μm order	cm-order	cm-order

In this research, in order to evaluate the performance of the amplifier-assisted CRDS, an EDFA (Erbium-doped fiber amplifier) is used in our experimental system to compensate the waveguide propagation loss.

1.3.3 Issues in amplifier-assisted CRDS

In our experimental system, an EDFA is set inside the closed loop of CRDS. EDFA in a closed loop; however; results in two serious issues.

The first issue is self-lasing. When EDFA is at a high pumping condition, ASE (amplified spontaneous emission) generated by EDFA loops inside the system and be amplified in the EDFA. Then, it starts self-lasing at a wavelength different from sensing light. Once self-lasing happens, sensing light looses the gain from EDFA. Without sufficient sensing light intensity, the sensing path length for ppm-order gas sensing is impossible to realize. Thus, self-lasing issue prevent ppm-order gas sensing.

The second issue is the amplifier noise issue. The amplifier noise [96] which exists at sensing light wavelength is hardly eliminated. In ppm-order gas sensing, the amplifier noise loops inside the system with sensing light for more than 1,000 times. The significant accumulated noise intensity may surpass the sensing light intensity and prevent ppm-order breath sensing. Hence, the accumulated noise intensity influences the sensing ability of amplifier-assisted CRDS system directly.

In this research, we have proposed the polarization direction control scheme to suspend the self-lasing. Based on our calculation, ppm-order gas sensing is available under the influence of the amplifier noise with sufficient injection light intensity. The details will be discussed in the next chapters.

1.4 Outline of this thesis

We discussed the integrated optical sensing circuit configuration in this thesis. This thesis consists of 5 chapters. In this 5 chapters, the optical sensing circuit configuration, the sensing principle, the issues of the sensing system and their solutions, and the sensing experiment results are introduced.

Chapter 1 explained the research background and purpose. The integrated optical sensing circuit configuration (amplifier-assisted CRDS system) was introduced.

Chapter 2 explained the sensing principle of the amplifier-assisted CRDS system.

Chapter 3 introduced the issues that were happened in the amplifier-assisted CRDS system. The reasons and the solutions of these two issues have been discussed. With the issues being improved, the calculation results showed that several kinds of ppm-order gases (CO_2, CH_4, NH_3, and CH_3COCH_3) are sensing-available by using the injection light intensity between 1mW and 50mW.

Chapter 4 showed the gas sensing experiment results. 3% CO2 was detected successfully.

In Chapter 5, the results that mentioned above have been summarized. The future view of the integrated sensing circuit has been discussed.

Reference

[1] World Health Organization, “Global health and ageing”, pp. 2-4 (2011).

[2] United Nations, Ageing issues: https://www.un.org/en/sections/issues-depth/ageing/.

[3] S. Ogura, and M. M. Jakovljevic, “Editorial: Global population aging-Health care, social and economic consequences”, Frontiers in public health, **6**, pp. 335 (2018).

[4] C. Zhao, D. D. Yu, K. Kang, Y. Liu, S. Q. Li, Z. Wang, H. Ji, B. C. Zhao, L. L. Ji, X. P. Leng, and J. W. Tian, “Role of contrast-enhanced ultrasound sonography in the medical diagnostics of the disease activity in patients with Takayasu arteritis”, IEEE Access, **7**, pp. 23240-23248 (2019).

[5] W. J. Manning, D. J. Atkinson, W. Grossman, S. Pauling, and R. R. Edelman, “First-pass nuclear magnetic resonance imaging studies using gadolinium-DTPA in patients with coronary artery disease”, Journal of the American College of Cardiology, **18** (4), pp. 959-965 (1991).

[6] G. H. Han, X. B. Liu, F. F. Han, I. N. T. Santika, Y. F. Zhao, X. M. Zhao, and C. W. Zhou, “The LISS – A public database of common imaging signs of lung diseases for computer-aided detection and diagnosis research and medical education”, IEEE Transactions on Biomedical Engineering, **62** (2), pp. 648-656 (2015).

[7] R. E. Gelder, C. Y. Nio, J. Florie, J. F. Bartelsman, P. Snel, S. W. Jager, S. J. Deventer, J. S. Lameris, P. M. M. Boossuyt, and J. Stoker, "Computed tomographic colonography compared with colonoscopy in patients at increased risk for colorectal cancer", Gastroenterology, **127**(1), pp. 41-48 (2004).

[8] C. A. Mair, A. R. Quinones, and M. A. Pasha, "Care preferences among middle-aged and older adults with chronic disease in Europe: individual health care needs and national health care infrastructure", The Gerontologist, **56** (4), pp.687-701 (2016).

[9] M. Velikova, R. L. Smeets, J. T. Scheltinga, P. J. F. Lucas, and M. Spaanderman, "Smartphone-based analysis of biochemical tests for health monitoring support at home", Healthcare Technology Letters, **1** (3), pp. 92-97 (2014).

[10] S. Tanaka, K. Motoi, M. Nogawa, T. Yamakoshi, and K. I. Yamakoshi, "Feasibility study of a urine glucose level monitor for home healthcare using near infrared spectroscopy", 2006 International Conference of the IEEE Engineering in Medicine and Biology Society, pp. 6001-6003 (2008).

[11] A. E. Burke, K. M. Thaler, M. Geva, and Y. Adiri, "Feasibility and acceptability of home use of a smartphone-based urine testing application among women in prenatal care", American Journal of

Obstetrics & Gynecology", **221** (5), pp. 527-528 (2019).

[12] X. W. Huang, Y. B. Li, J. Chen, J. X. Liu, R. J. Wang, X. F. Xu, J. F. Yao, and J. H. Guo, "Smartphone-based blood lipid data acquisition for cardiovascular disease management in internet of medical things", IEEE Access, **7**, pp. 75276-75283 (2019).

[13] OMRON blood pressure monitoring device: https://www.healthcare.omron.co.jp/corp/news/2019/1024.html.

[14] OMRON blood glucose monitoring device: https://www.omron.co.jp/press/2008/04/h0415.html.

[15] S. R. Steinhubl, J. Waalen, A. M. Edwards, L. M. Ariniello, R. R. Mehta, G. S. Ebner, C. C. Pharm, K. B. Motes, E. Felicione, T. Sarich, and E. J. Topol, "Effect of a home-based wearable continuous ECG monitoring patch on detection of undiagnosed atrial fibrillation: the mSToPS randomized clinical trial", Jama, **320** (2), pp. 146-155 (2018).

[16] N. Marczin, *Disease Markers in Exhaled Breath*, M. Yacoub, ed., Marcel Dekker, New York (2003) Chap. 1.

[17] C. Wang, and P. Sahay, "Breath analysis using laser spectroscopic techniques: breath biomarkers, spectral fingerprints, and detection limits", Sens., **9**(10), 8230-8262 (2009).

[18] M. Sawano, "Basics and medical applications of breath analysis", Japan Air Cleaning Association, **54** (5), pp. 329-332 (2017). [in Japanese].

[19]B. J. Novak, D. R. Blake, S. Meinardi, F. S. Rowland, A. Pentello, D. M. Cooper, and P. R. Galassetti, “Exhaled methyl nitrate as a noninvasive marker of hyperglycemia in type 1 diabetes”, Proceedings of the National Academy of Science, **104** (40), pp. 15613-15618 (2007).

[20]P. R. Galassetti, B. Novak, D. Nemet, C. R. Gottron, D. M. Cooper, S. Meinardi, R. Newcomb, F. Zaldivar, and R. Blake, “Breath ethanol and acetone as indicators of serum glucose levels: an initial report”, Diabetes technology & Therapeutics, **7** (1), pp. 115-123 (2005).

[21]M. Phillips, R. N. Cataneo, T. Cheema, and J. Greenberg, “Increased breath biomarkers of oxidative stress in diabetes mellitus”, Clinica Chimica Acta, **334** (1-2), pp. 189-194 (2004).

[22]D. Roccarina, E. C. Lauritano, M. Gabrielli, F. Franceschi, V. Ojetti, and A. Gasbarrini, “The role of methane in intestinal disease”, The American journal of gastroenterology, **105** (6), pp.1250-1256 (2010).

[23]A. B. Sahakian, S. R. Lee, and M. Pimetel, “Methane and the gastrointestinal tract”, Digestive diseases and sciences, **55** (8), pp.2135-2143 (2010).

[24]M. Pimentel, A. G. Mayer, S. Park, E. J. Chow, A. Hasan, and Y. Kong, “Methane production during lactulose breath test is associated with gastrointestinal disease presentation”, Digestive Diseases and Science, **48** (1), pp. 86-92 (2003).

[25]S. W. Ryter, and A. MK. Choi, “Therapeutic applications of carbon monoxide in lung disease”, Current opinion in pharmacology, **6** (3), pp. 257-262 (2006).

[26]K. Zayasu, K. Sekizawa, S. Okinaga, M. Yamaya, T. Ohrui, and H. Sasaki, “Increased carbon monoxide in exhaled air of asthmatic patients”, American Journal of respiratory and Critical Care Medicine, **156** (4), pp. 1140-1143 (1997).

[27]P. Paredi, W. Biernacki, G. Invernizzi, S. A. Kharitnov, and P. J. Barnes, “Exhaled carbon monoxide levels elevated in diabetes and correlated with glucose concentration in blood: a new test for monitoring the disease?”, Chest, **116** (4), pp.1007-1011 (1999).

[28]H. Zan, W. Tsai, Y. Lo, Y. Wu, and Y. Yang, “Pentacene-based organic thin film transistors for ammonia sensing”, IEEE Sensors Journal, **12**(3), pp.594-601 (2011).

[29]S. A. Kharitonov, K. Rajakusasingam, B. O’Connor, S. R. Durham, and P. J. Barnes, “Nasal nitric oxide is increased in patients with asthma and allergic rhinitis and may be modulated by nasal glucocorticoids”, Journal of allergy and clinical immunology, **99** (1), pp. 58-64 (1997).

[30]K. Kao, M. Hsu, Y. Chang, S. Gwo, and J. Andrew Yeh, “A sub-ppm acetone gas sensor for diabetes detection using 10nm thick ultrathin InN FETs”, Sensors, **12** (6), pp.7157-7168 (2012).

[31]C. Turner, C. Walton, S. Hoashi, and M, Evans, “Breath acetone concentration decreases with blood glucose concentration in type 1 diabetes mellitus patients during hypoglycaemic clamps”, Journal of breath research, **3** (4), pp.046004 (2009).

[32]Y. Yamada, and S. Hiyama, “Breath acetone analyzer to achieve “Biochip mobile terminal”. NTT DOCOMO Technology, **14** (1), pp. 51-57 (2012).

[33]M. Refat, T. J. M, M. Kazui, T. H. Risby, J. A. Perman, and K. B. Schwarz, “Utility of breath ethane as a noninvasive biomarker of vitamin E status in children”, Pediatric Research, **30** (5), pp. 396 (1991).

[34]C. A. Riely, G. Cohen, and M. Lieberman, “Ethane evolution: a new index of lipid peroxidation”, Science, **183** (4121), pp. 208-210 (1974).

[35]G. D. Lawrence, and G. Cohen, “Ethane exhalation as an index of in vivo lipid peroxidation: Concentrating ethane from a breath collection chamber”, Analytial Biochemistry, **122** (2), pp. 283-290 (1982).

[36]T. H. Risby, and S. F. Solga, “Current status of clinical breath analysis”, Applied Physics B: Lasers and Optics, Springer Berlin / Heidelberg, **85** (2-3), pp. 421-426 (2006).

[37]P. Li, E. Li, G. Xu, C. Wang, Y. Guo, and Y. He, “Breath pentane: an indicator for early and continuous monitoring of lipid peroxidation in hepatic ischaemia-reperfusion injury”, European Journal of

Anaesthesiology, **26** (6), pp. 513-519 (2009).

[38]I. Horvath, W. Macnee, F. J. Kelly, P. N. R. Dekhuijzen, M. Philips, G. Doring, A. M. K. Choi, M. Yamaya, F. H. Bach, D. Willis, L. E. Donnelly, K. F. Chung, and J. Barnes, "Haemoxygenase-1 induction and exhaled markers of oxidative stress in lung diseases", European Respiratory Journal, **18** (2), pp. 420-430 (2001).

[39]K. Kostikas, G. Papatheodorou, K. Psathakis, P. Panagou, and S. Loukides, "Oxidative stress in expired breath condensate of patients with COPD", Chest, **124** (4), pp. 1373-1380 (2003).

[40]A. Antczak, "Markers of oxidative stress in exhaled breath condensate, NATO Science Series, Series.**1**, pp. 333-337 (2002).

[41]E. C. Lases, V. A. M. Duurkens, W. B. M. Geritsen, and F. J. L. M. Haas, "Oxidative stress after lung resection therapy: a pilot study", Chest, **117** (4), pp. 999-1003 (2000).

[42]C. M. F. Kneepkens, G. Lepage, and C. C. Roy, "The potential of the hydrocarbon breath test as a measure of lipid peroxidation", Free Radical Biology and Medicine, **17** (2), pp. 127-160 (1994).

[43]Otsuka pharmaceutical: https://www.otsuka.co.jp/health-and-illness/h-pylori/tests-and-eradication/.

[44]Anima: https://anima.jp/products/at1100a/.

[45]Horiba: http://www.horiba.com/jp/process-environmental/products-jp/combustion-process/research-purpose/details/va-5000-va-5000wm-multi-component-gas-analyzer-31115/.

[46]Tiger optics: https://www.tigeroptics.com/product/prismatic-2.html.

[47]R. Takasu, “Compact sensor for environmental monitoring”, Fujitsu, **61**(1), pp. 47-51 (2010).[in Japanese]

[48]O. Tsuboi, S. Momose, and R. Takasu, Mobile sensor that quickly and selectively measures ammonia gas components in breath, Fujitsu Sci. Tech., **53**(2), pp. 38-43 (2017).

[49]T. Itoh, D. Nagai, and W. Shin, “Development of sensor device for breath analysis”, Sansouken Today, pp. 12-13 (2013).[in Japanese]

[50]H. Wakana, M. Yamada, and M. Sakairi, Portable alcohol detection system with breath- recognition function, 2018 IEEE Sensors. IEEE, pp. 1-4 (2018).

[51]G. Yoshikawa, T. Akiyama, S. Gautsch, P. Vettiger, and H. Rohrer, Nanomechanical membrane-type surface stress sensor, Nano Lett., **11**(3), pp. 1044-1048 (2011).

[52]F. Loizeau, H. Lang, T. Akiyama, S. Gautsch, P. Vettiger, A. Tonin, G. Yoshikawa, C. Gerber, and N. Rooij, Piezoresistive membrane-type surface stress sensor arranged in arrays for cancer diagnosis through

breath analysis, 2013 IEEE 26th International Conference on MEMS. IEEE, pp. 621-624 (2013).

[53]H. Miki, F. Matsubara, S. Nakashima, S. Ochi, K. Nakagawa, M. Matsuguchi, and Y. Sadaoka, A fractional exhaled nitric oxide sensor based on optical absorption of cobalt tetraphenylporphyrin derivatives. Sensors and Actuators B: Chemical, **231**, pp. 458-468 (2016).

[54]S. Tao, J. C. Fanguy, and T. V. S. Sarma, A fiber-optic sensor for monitoring trace ammonia in high-temperature gas samples with a CuCl2- doped porous silica optical fiber as a transducer, IEEE Sensors Journal, **8**(12), pp. 2000-2007 (2008).

[55]H. Gatty, G. Stemme, and N. Roxhed, A miniaturized amperometric hydrogen sulfide sensor applicable for bad breath monitoring, Micromachines, **9**(12), pp. 612 (2018).

[56]M. E. Achhab, and K. Schiebaum, Gas sensor based on plasma-electrochemically oxidized titanium foils, Journal of Sensors and Sensor Systems, **5**, pp. 273-281 (2016).

[57]P. Sanchez, C. Zamarreno, M Hernaez, I. Matias, and F. Arregui, Exhaled breath optical fiber sensor based on LMRs for respiration monitoring, Sensors, 2014 IEEE, pp. 1142-1145 (2014).

[58]T. Iwata, T. Katagiri, and Y. Matsuura, Real-time analysis of isoprene in breath by using ultraviolet-absorption spectroscopy with a hollow

optical fiber gas cell, Sensors, **16**(12), pp. 2058 (2016).

[59]R. Ueno, K. Ishii, K. Suzuki, and H. Funaki, Infrared multispectral imaging with silicon-based multiband pass filter and infrared focal plane array, 2015 9th International Conference on Sensing Technology (ICST). IEEE, pp. 211-214 (2015).

[60]L. Tombez, E. Zhang, J. Orcutt, S. Kamlapurkar, and W. Green, Methane absorption spectroscopy on a silicon photonic chip, Optica, **4**(11), pp. 1322-1325 (2017).

[61]K. Namjou, C. B. Roller, T. E. Reich, J. D. Jeffers, G. L. Mcmillen, P. J. Mccann, M. A. Camp, Determination of exhaled nitric oxide distributions in a diverse sample population using tunable diode laser absorption spectroscopy, Applied Physics B, **85**, pp. 427-435 (2006).

[62]M. B. Frish, Current and emerging laser sensors for greenhouse gas sensing and leak detection, Next-Generation Spectroscopic Technologies VII. International Society for Optics and Photonics, **9101**, pp. 91010H (2014).

[63]M. Murtz, D. Kleine, S. Stry, H. Dahnke, P. Hering, J. Lauterbach, K. Kleinermanns, W. Urban, H. Ehlers, and D. Ristau, “Ultra-sensitive trace gas monitoring with a CW Ring-down spectrometer”, Environmental Science and Pollution Research Special, **4**, pp. 61-67 (2002).

[64]M. Murtz, D. Halmer, M. Horstjann, S. Thelen, P. Hering, “ Ultra

sensitive trace gas detection for biomedical applications", Spectrochimica Acta Part A, **63**, pp. 963-969 (2005).

[65] K. Bodenhofer, A. Hierlemann, G. Noetzel, U. Weimar, and W. Gopel, "Performances of mass-sensitive devices for gas sensing: Thickness shear mode and surface acoustic wave transducers", Analytical Chem., **68**(13), pp. 2210-2218 (1996).

[66] K. Reddy, Y. Guo, J. Liu, W. Lee, M. K. K. Oo, and X. Fan, "On-chip fabry-perot interferometric sensors for micro-gas chromatography", Sensors and Actuators B: Chem., **159**(1), pp. 60-65 (2011).

[67] T. Iwata, T. Katagiri, and Y. Matsuura, "Real-time analysis of isoprene in breath by using ultraviolet-absorption spectroscopy with a hollow optical fiber gas cell", Sens., **16**(12), 2058 (2016).

[68] L. Tombez, E. Zhang, J. Orcutt, S. Kamlapurkar, and W. Green, "Methane absorption spectroscopy on a silicon photonic chip", Opt., **4**(11), 1322-1325 (2017).

[69] K. Namjou, C. B. Roller, T. E. Reich, J. D. Jeffers, G. L. Mcmillen, P. J. Mccann, and M. A. Camp, "Determination of exhaled nitric oxide distributions in a diverse sample population using tunable diode laser absorption spectroscopy", App. Phys. B, **85**, 427-435 (2006).

[70] H. Dahnke, D. Kleine, P. Hering, and M. Murtz," Real-time monitoring of ethane in human breath using mid-infrared cavity leak-out spectroscopy", Appl. Phys. B, **72**(8), 971-975 (2001).

[71] N. Gayraud, L. W. Kornaszewski, J. M. Stone, J. C. Knight, D. T. Reid, D. P. Hand, and W. N. MacPherson, "Mid-infrared gas sensing using a photonic bandgap fiber", App. Opt., **47**(9), 1269-1277 (2008).

[72] R. E. Huffman, "Absorption cross-sections of atmospheric gases for use in aeronomy", Can. J. of Chem., 47(10), pp. 1823-1834 (1969).

[73] HITRAN Database: http://www.cfa.harvard.edu/hitran/.

[74] A. Barth, "Infrared spectroscopy of proteins", Biochim. et Biophys. Acta-Bioenerg., **1767**(9), 1073-1101 (2007).

[75] W. Lai, S. Chakravarty, X. Wang, C. Lin, and R. Chen, "On-chip methane sensing by near-IR absorption signatures in a photonic crystal slot waveguide", Opt. Lett., **36**(6), 984-986 (2011).

[76] S. S. Kim, C. Young, B. Vidakovic, S. G. A. Gabram-Mendola, C. W. Bayer, and B. Mizaikoff, "Potential and challenges for mid-infrared sensors in breath diagnostics" IEEE Sens. J., **10**(1), 145-158 (2010).

[77] A. Wilk, F. Seichter, S. Kim, E. Tutuncu, B. Mizaikoff, J.A. Vogt, U. Wachter, and P. Radermacher "Toward the quantification of the $^{13}CO_2/^{12}CO_2$ ratio in exhaled mouse breath with midinfrared hollow waveguide gas sensors", Anal. Bioanal. Chem., **402**(1), 397-404 (2012).

[78] M. Tsujino, H. Hokazono, J. Chen, and K. Hamamoto, “Optical amplifier assisted cavity ring down spectroscopy (CRDS) method for compact infrared sensing”, Tech. Dig. MOC, **H57**, 1-2 (2013).

[79] A. K. Chu, and S. F. Hong, “Buried sol-gel/SiON waveguide structure for passive alignment to single-mode fiber on Si substrate”, IEEE Photonics Tech. Lett., **19**(1), pp. 45-47 (2007).

[80] Y. Zhou, V. Karagodsky, B. Pesala, F. G. Sedgwick, and C. J. Chang-Hasnain, “A novel ultra-low loss hollow-core waveguide using subwavelength high-contrast gratings”, Opt. Express, **17**(3), pp. 1508-1517 (2009).

[81] R. Bicknell, L. King, C. E. Otis, J. S. Yeo, N. Meyer, P. Kornilovitch, S. Lerner, and L. Seals, “Fabrication and characterization of hollow metal waveguides for optical interconnect applications”, Appl. Phys. A, **95**(4), pp. 1059-1066 (2009).

[82] C. Shi, C. Lu, C. Gu, L. Tian, R. Newhouse, S. Chen, and J. Z. Zhang, “Inner wall coated hollow core waveguide sensor based on double substrate surface enhanced Raman scattering”, Appl. Phys. Lett., **93**(15), pp. 153101-3 (2008).

[83] T. Alasaarela, D. Korn, L. Alloatti, A. Saynatjoki, A. Tervonen, R. Palmer, J. Leuthold, W. Freude, and S. Honkanen, “Reduced propagation loss in silicon strip and slot waveguides coated by atomic

layer deposition", Opt. Express, **19**(12), pp. 11529-11538 (2011).

[84] R. Ding, T. Baehr-Jones, W. J. Kim, X. Xiong, R. Bojko, J. M. Fedeli, M. Fournier, and Michael Hochberg, "Low-loss strip-loaded slot waveguides in Silicon-on-Insulator", Opt. Express, **18**(24), pp. 25061-25067 (2010).

[85] R. Ding, T. Baehr-Jones, W. Kim, B. Boyko, R. Bojko, A. Spott, A. Pomerene, C. Hill, W. Reinhardt, and M. Hochberg, "Low-loss asymmetric strip-loaded slot waveguides in silicon-on-insulator", Appl. Phys. Lett., **98**(23), pp. 233303 (2011).

[86] J. T. Robinson, L. Chen, and M. Lipson, "On-chip gas detection in silicon optical microcavities", Opt. Express, **16**(6), pp. 4296-4301 (2008).

[87] J. Chen, H. Hokazono, D. Nakashima, M. Tsujino, Y. Hashizume, M. Itoh, and K. Hamamoto, "Low loss silica high-mesa waveguide for infrared sensing", Jpn. J. of App. Phys., **53**(2), 022502 (2014).

[88] I. Alam, Y. Matsunaga, S. Hirofuji, T. Mitomi, T. Murayama, Y. Kokaze, H. Wado, Y. Takeuchi, and K. Hamamoto, "Low loss high-mesa Si/SiO2 wire waveguides fabricated using neutral loop discharge plasma etching for infrared absorption spectroscopy",15th Microoptics Conference, **F3** (2009).

[89] T. Claes, J. G. Molera, K. D. Vos, E. Schacht, R. Baets, and P. Bienstman, "Lable-Free Biosensing With a Slot-Waveguide-Based Ring Resonator

in Silicon on Insulator", IEEE Photonics J., **1**(3) (2009).

[90] S. Wu, A. Deev, M. Haught, and Y. Tang, "Hollow waveguide quantum cascade laser spectrometer as an online microliter sensor for gas chromatography", J. of Chromatography A, **1188**, pp. 327-330 (2008).

[91] Y. Han, W. Y. Li, H. S. Jiang, and K. Hamamoto, "Significant propagation loss reduction on silicon high-mesa waveguides using thermal oxidation technique", 24th OptoElectronics and Communications Conference, **P47**, pp, 1-3 (2019).

[92] J. Chen, H. Hokazono, M. Tsujino, D. Nakashima, and K. Hamamoto, "Proposal of multiple-slot silica high-mesa waveguide for infrared absorption", IEICE Electronics Express, **10**, pp. 20130871 (2013).

[93] INVOCOM: Optical amplifiers: classification, basic configurations and principles of operation: www.invocom.et.put.poznan.pl/

[94] M. J. Connolly, *Semiconductor Optical Amplifiers*, Springer-Verlag, Boston (2002) Chap.1.

[95] W. Y. Li, Y. Han, Z. H. Chen, H. S. Jiang, and K. Hamamoto, "Amplifier-assisted CRDS (cavity ring-down spectroscopy) toward compact breath sensing", Jpn. J. of App. Phys., **58**(SJ), SJJD01 (2019).

[96] Ter-Mikirtychev, and Vartan, *Fundamentals of fiber lasers and fiber amplifiers*, Springer, Swizerland (2014) Chap. 7.

Chapter 2

Breath sensing principle and sensing circuit configuration

2.1 Introductory overview

Home-base breath sensors are expected to present characteristics such as hand-held size, and several breath contents sensing at the same time. As mentioned in section 1.2, infrared absorption spectroscopy is capable for several kinds of gases sensing. Meanwhile, using waveguide as the sensing path based on CRDS (cavity ring-down spectroscopy) realizes hand-held size sensor. In this chapter, we firstly explain the principle of infrared absorption spectroscopy and CRDS in section 2.2. Then, we introduce the sensing circuit configuration with waveguide in section 2.3. Finally, the conclusions are summarized in section 2.4.

2.2 Breath sensing principle

2.2.1 Infrared absorption spectroscopy

In general, a volatile gas (target gas) has its own eigen absorption wavelength at infrared band [1-3]. The amount of the absorbed infrared light intensity is

related to the density of the gas molecule N' [molecule/cm^3], the gas absorption cross-section σ [cm^2/molecule], and the interaction length L [cm] between sensing light and the target gas. The relationship of the light intensity, N', σ, and L is expressed as [4]:

$$I_{out}/I_{in} = \exp(\sigma N' L) \quad (2.1).$$

Here, I_{in} [mW] and I_{out} [mW] are the injection and the output light intensity, respectively.

The density of the gas molecule N' [molecule/cm^3] is expressed as [5]:

$$N' = \frac{NA \times n}{V_{total}} \quad (2.2).$$

NA [number/mol] is Avogadro constant [6]. In breath sensing, n [mol] is the amount of the target gas. V_{total} [cm^3] is the total volume of the breath. Gas concentration N [ppm] is expressed by V_{total} and the volume of the target gas V_{gas} [l]as:

$$N = \frac{V_{gas}}{V_{total}} \times 10^{-9} \quad (2.3).$$

Based on the Ideal gas law [7] which is

$$PV_{gas} = nRT \quad (2.4),$$

The density of the gas molecule N' could be express by gas concentration N as:

$$N' = \frac{P \times NA}{RT} \times N \times 10^{-9} \quad (2.5).$$

Here, P [atm] is pressure, T [K] is temperature, R [l^3·atm/mol·K] is Ideal gas constant.

Therefore, the sensing light intensity has a relationship with gas concentration N as:

$$I_{out}/I_{in} = \exp\left(\sigma L \times N \times \frac{P \times NA \times 10^{-9}}{RT}\right) \quad (2.6).$$

To measure ppm-order gases in exhaled breath by using infrared absorption spectroscopy, the sufficient gas absorption (typically 3 dB) is desired [8]. We set the criteria of "3 dB difference" between I_{out} and I_{in} to estimate the necessary interaction length L for some ppm-order breath contents. The estimated results are summarized in Tab. 2.1, with the breath content names, their absorption cross-section σ, absorption wavelength λ [μm], the related disease [9-14], and the needed interaction length L [km] for sensing their concentration N [ppm] in exhaled breath.

Tab. 2.1 ppm-order breath components and their needed sensing path length. The required sensing path length are all at km-order.

Breath content	λ [μm]	N [ppm]	σ [cm^2/molecule]	Related disease	L [km]
Methane (CH_4)	1.65	2-10	1.6×10^{-20}	Intestine disease	20
Ammonia (NH_3)	1.51	0.5-5	2.5×10^{-20}	Liver disease	25
Acetone (CH_3COCH_3)	1.68	1.7-3.7	3.6×10^{-22}	Diabetes	2309
Carbon monoxide (CO)	1.57	3.3-5.4	2.2×10^{-23}	Diabetes	27957

As shown in Tab. 2.1, km-order length of sensing path is needed for the ppm-order gas concentration detection in exhaled breath by using infrared absorption spectroscopy. This extremely long sensing path is impossibly

realized in hand-held size sensor.

2.2.2 CRDS system

To reduce the km-order length sensing path down to below 1 m, one attractive technique is known as CRDS method [15, 16]. Figure 2.1 shows the schematic configuration of the general CRDS system. The gas-cell has high reflection mirrors at the both ends of the gas-cell [17, 18]. The high reflection mirrors are used to reflect the sensing light inside the gas-cell. When the reflection happens for more than 1,000 times in a 1 m length gas-cell for instance, the corresponding sensing path length reaches to the effective length of km-order. During each reflection, slight portion of the not-reflected (therefore transmitted) light leaks out from the gas-cell through the high reflection mirror. The measurement is carried to detect this leak-out light intensity. The example measurement result (light intensity as a function of time) is shown in the right-hand side of Fig. 2.1. The light intensity decreases because of the leak-out light from the mirror at the gas-cell ends. This situation happens even for "no-gas in gas-cell" situation. In the situation of "gas in gas-cell", the light intensity decreases faster than the case of "no-gas" due to the gas absorption. Here, the cavity ring-down time [19] τ and τ_{gas} are defined as follows: the time that light intensity decreases to the criteria level (normally 1/e) [20, 21] (black dash-line in Fig. 2.1). And τ and

τ_{gas} are the cavity ring-down times for "no-gas in gas-cell" and "gas in gas-cell" situation, respectively.

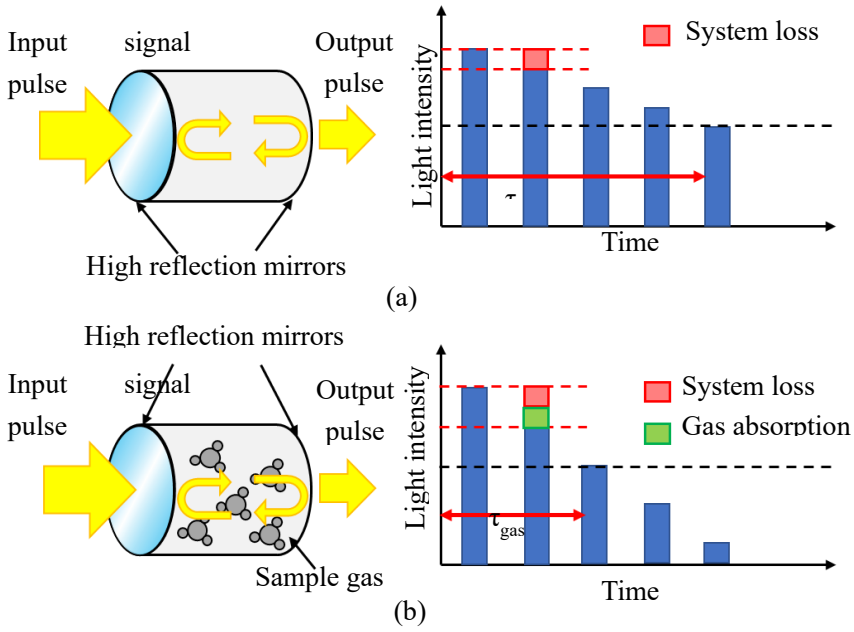

Fig. 2.1 Schematic configuration of the general CRDS system with (a) no gas in cavity and (b) sample gas in cavity. The output pulse light intensity decreases fast in "gas in cavity" situation than "no gas" situation because of the gas absorption. The gas concentration is estimated by using the time of τ and τ_{gas}. τ and τ_{gas} are the time that the light intensity decreases to the set light intensity criteria.

As shown in the right-hand side of the Fig. 2.1, the leak-out light intensity is exponential decay as a function of time [22-24]. At time is t [s], the leak-out light intensity is:

$$I_{out} = \exp\left[-\left(\frac{1}{\tau_0}\right) \times t\right] \qquad (2.7).$$

τ_0 is the decay life of the light in gas-cell. In the "no-gas in gas-cell" situation, τ_0 equals to the ring-down time τ. And in the "gas in gas-cell" situation, τ_0 equals to the ring-down time τ_{gas}. So, the leak-out light intensity in "no-gas" and "gas in gas-cell" situation are:

$$I_{out} = \exp\left[-\left(\frac{1}{\tau}\right) \times t\right] \quad \text{(no-gas)} \tag{2.8},$$

and

$$I_{out} = \exp\left[-\left(\frac{1}{\tau_{gas}}\right) \times t\right] \quad \text{(gas in gas-cell)} \tag{2.9},$$

respectively.

In “gas in gas-cell” situation, the light intensity decreases because of 2 reasons: (1) the leak-out light from the mirror at the gas-cell ends, and (2) the gas absorption. (1) is expressed as $\exp\left[-\left(\frac{1}{\tau}\right) \times t\right]$. (2) is expressed as $\exp(-\sigma N' c)$ based on eq. (2.1). c [cm/μs]is the light speed. Hence, eq. (2.9) could be written as:

$$I_{out} = \exp\left[-\left(\frac{1}{\tau} + \sigma N' c\right) \times t\right] \tag{2.10}.$$

By calculating the eq. (2.9) and eq. (2.10), we got

$$\triangle\left(\frac{1}{\tau}\right) = \frac{1}{\tau_{gas}} - \frac{1}{\tau} = \sigma N' c$$

$$= \sigma c \times N \times \frac{P \times NA \times 10^{-9}}{RT} \tag{2.11}.$$

Equation 2.11 shows that the target gas concentration N [ppm] could be estimated by using the cavity ring-down times as:

$$N = \left(\frac{1}{\tau_{gas}} - \frac{1}{\tau}\right) \times \frac{RT}{\sigma c \times P \times NA \times 10^{-9}} \tag{2.12}.$$

Based on the analysis above, CRDS system is capable for ppm-order gas sensing.

2.3 Amplifier-assisted waveguide CRDS configuration

CRDS system realizes the corresponding km-order sensing path in a gas-cell. The problem of general CRDS as hand-held sensor is its large gas-cell size. To realize hand-held sensor, we proposed high-mesa waveguide as the optical sensing path instead of the gas-cell. This is because waveguide has a potential of integrating a long optical path in a compact area. When sensing light propagates in the high-mesa waveguide, a portion of light goes out of the waveguide. This portion of light intensity is used for gas absorption. Gas absorption happens by using waveguide as the sensing path. Hence, waveguide with high-reflection films on both facets is suitable in CRDS instead of general gas-cell for hand-held sensor.

The structure of waveguide CRDS is shown in Fig. 2.2. As shown in this figure, several meter length waveguide is coiling on the chip. The waveguide has high-reflection films [25] on both facets. Sensing light is reflected rapidly inside the waveguide. The portion of light coming out from waveguide is being absorbed by gas. One problem is that, waveguide has propagation loss. Most of the injected sensing light is reduced due to the propagation loss. As mentioned in section 1.2.1, the silica high-mesa waveguide has a propagation loss of 0.02 dB/cm. When light propagates in a 1 m length silica high-mesa waveguide for instance, light intensity decreases 2 dB. If light reflecting inside the silica high-mesa waveguide

exceeds 1,000 times for ppm-order gas sensing, the accumulated loss may reach to 2,000 dB. Breath sensing is impossible with this huge loss.

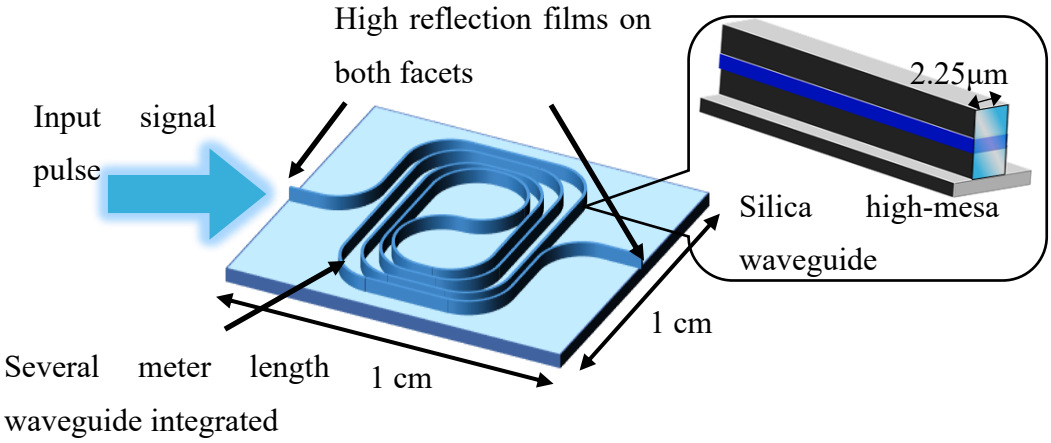

Fig. 2.2 Waveguide CRDS schematic configuration. Several meter length waveguide is integrated on a 1 cm × 1 cm size chip. The waveguide has high-reflection films on both facets. The structure of waveguide with high-reflection films corresponds to a several meter length CRDS gas-cell.

To solve this problem, we proposed amplifier-assisted CRDS. The configuration of amplifier-assisted waveguide CRDS is shown in Fig. 2.3. In amplifier-assisted CRDS, waveguide has no high-reflection film. The sensing light at the outbound of the waveguide is guided to an optical amplifier to compensate the waveguide propagation loss. After amplification, the sensing light is leaded to the inbound of the waveguide. This waveguide configuration; however; enclose the sensing light into a loop without leak-out light. It is impossible; therefore; to monitor the leak-out light intensity decrease as CRDS.

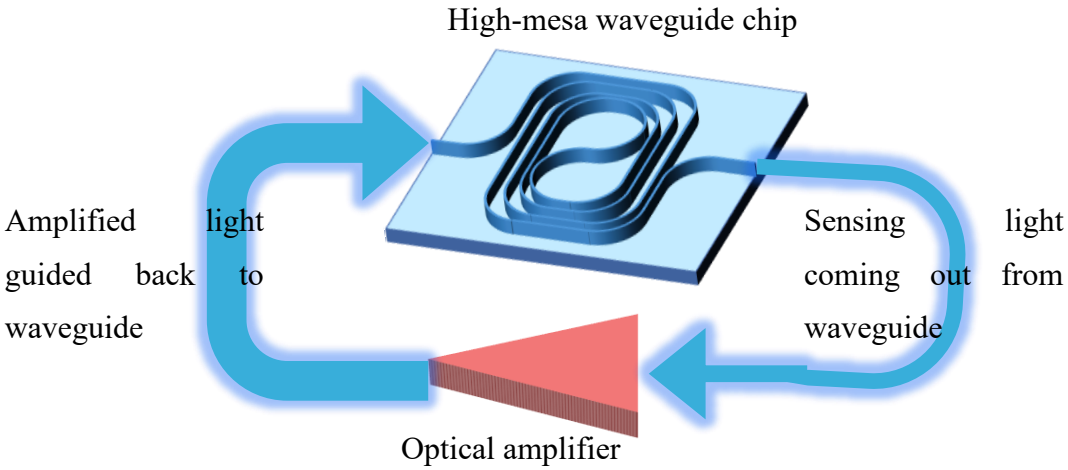

Fig. 2.3 Amplifier-assisted waveguide CRDS schematic configuration. Optical amplifier is used to compensate the waveguide propagation loss. The amplified sensing light is guided back to waveguide for gas absorption.

As a solution, optical couplers are used to connect the output port of the amplifier and the inbound of the waveguide. One of the candidates of the optical amplifier is SOA (semiconductor optical amplifier). This is because SOA is capable for integrating. To evaluate the performance of the amplifier in CRDS system, we used an EDFA (Erbium-doped fiber amplifier) in the experiment. The experimental set-up of amplifier-assisted CRDS is shown in Fig. 2.4. In this experimental set-up, an EDFA is set inside the CRDS to demonstrate the effectiveness of the amplifier-assisted CRDS. Two optical couplers are used to guide the sensing light. The injected sensing light-pulse is guided to the inbound of the waveguide via coupler 1. The light coming out from the outbound of the waveguide is amplified by EDFA. Then, most of the sensing light is leaded back to the inbound of the waveguide via

coupler 2 and 1. A portion of "leak-out light" is monitored via one output branch of the coupler 2. The amount of leak-out light is controlled by the branch ratio [26] of coupler 2.

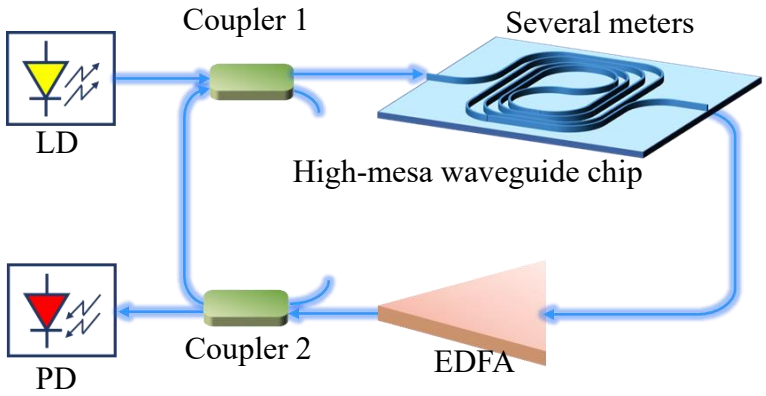

Fig. 2.4 Experimental system of amplifier-assisted waveguide CRDS. Coupler 1 is used to guide the sensing light into the sensing waveguide. Coupler 2 is used to lead the "leak-out" light to PD and guide most of the sensing light back to the sensing waveguide.

In this experiment, sensing light is at 1572 nm wavelength. This wavelength is the absorption wavelength of CO_2, which is a major content in human breath. Figure 2.5 are the amplifier-assisted CRDS results (light intensity as a function of time when the injected light intensity was 1 mW). The orange pulse-trains correspond to the result of "before amplification" situation. The blue pulse-trains correspond to the result of "after amplification" situation. Without amplification, light intensity decreased immediately. It only looped in waveguide for 3 times. When EDFA provided 5 dB gain and compensated part of the propagation loss, the looping time increased to 16 from only a few. These results lead to the sensing path length

extending more than 5 times than that without amplification.

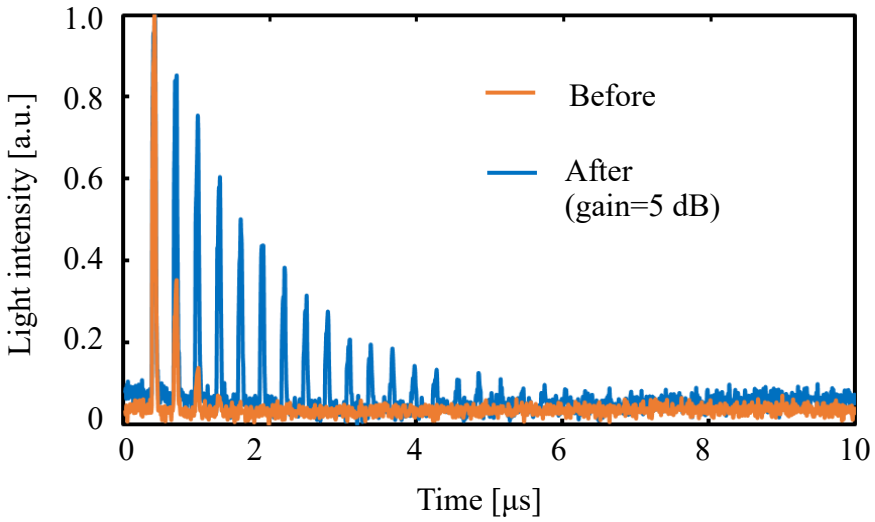

Fig. 2.5 Experiment results of amplifier-assisted waveguide CRDS, before and after amplification. With amplifier gain of 5 dB, pulse number in the pulse-train increased to 16 from a few. This result corresponds to the sensing path length extending more than 5 times than that without amplification.

In amplifier-assisted waveguide CRDS, gas concentration is estimated by the cavity ring-down time. As shown in Fig. 2.5, cavity ring-down time is related to the number of the pulses. So, we need to estimate how many pulses are needed for ppm-order gas sensing.

At the situation of "no-gas", the light intensity of the last pulse in pulse-train I_{out} is:

$$I_{out} = I_{in} \times [G \times Loss_{(system)}]^m \qquad (2.13).$$

And at the situation of "with gas", the light intensity of the last pulse in pulse-train $I_{out\ (gas)}$ is:

$$I_{out\ (gas)} = I_{in} \times [G \times Loss_{(system)} \times Loss_{(abs.)}]^{m(gas)} \quad (2.14).$$

I_{in} is the injection light intensity. G is the amplifier gain. $Loss_{(system)}$ indicates the system loss, including the waveguide propagation loss and the couplers losses. $Loss_{(abs.)}$ is the gas absorption loss. m and $m_{(gas)}$ are the required number of pulses at the situation of "no-gas" and "with gas", respectively. When the pulse intensity reaches to the criteria level (normally 1/e), we have:

$$I_{out} = I_{out\ (gas)} \quad (2.15).$$

To distinguish the cavity ring-down time difference between "no-gas" and "with gas" situation, the minimum difference between m and $m_{(gas)}$ is

$$m = m_{(gas)} + 1 \quad (2.16).$$

By using the condition of eq. 2.15 and eq. 2.16, we summarized eq.2.13 and eq. 2.14 as:

$$[G \times Loss_{(system)}]^{m(gas)+1} = [G \times Loss_{(system)} \times Loss_{(abs.)}]^{m(gas)} \quad (2.17).$$

Thus, the required number of pulses $m_{(gas)}$ is calculated as:

$$m_{(gas)} = \log_{Loss(abs.)}^{G \times Loss_{(system)}} \quad (2.18).$$

Based on eq. 2.6, Loss (abs.) is expressed as

$$Loss_{(abs.)} = \exp\left(-\sigma \times N \times \frac{P \times NA \times 10^{-9}}{RT} \times L \times \Gamma_{air}\right) \quad (2.19).$$

As mentioned in section 1.2.1, Γ_{air} [%] is the portion of light intensity out from waveguide. The waveguide length L could be expressed by the

waveguide total loss $Loss_{(waveguide)}$ and waveguide propagation loss α as:

$$L = \frac{Loss_{(waveguide)}}{\alpha} \quad (2.20).$$

By using the waveguide performance evaluation constant *FOM* in eq. 1.2, the part of "$L\times \Gamma_{air}$" in eq. 2.19 could be expressed by *FOM* as:

$$L\times \Gamma_{air} = Loss_{(waveguide)} \times FOM \quad (2.21).$$

Thus, the waveguide length L is not needed in the estimation. The gas absorption loss $Loss_{(abs.)}$ could be estimated by setting the total waveguide loss $Loss_{(waveguide)}$ and the waveguide performance constant *FOM* as:

$$Loss_{(abs.)} = \exp\left(-\sigma\times N \times \frac{P\times NA\times 10^{-9}}{RT} \times Loss_{(waveguide)} \times FOM\right) \quad (2.22).$$

Human exhaled breath contains 4% CO_2. Thus, for instance, we estimate the necessary pulse number for 4% (40000 ppm) CO_2 by using the amplifier-assisted waveguide CRDS. The *FOM* of silica high-mesa waveguide is 1.35. The total waveguide loss is set as 20 dB. This total waveguide loss indicates a silica high-mesa waveguide length is 10 m. The gain of the amplifier is set as 20 dB. This gain totally compensates the waveguide loss. The system loss is set as 20.5 dB. This system loss includes 20 dB waveguide loss, and 0.5 dB coupler loss (a 99:1 coupler and a 90:10 coupler). The gas absorption loss

$$Loss_{(abs.)} = \exp\left(-7.7\times 10^{-23} \times 40000\times \frac{6.02\times 10^{23}\times 10^{-9}}{0.082\times 298} \times 20\times 1.35\right) \quad (2.23).$$

$Loss_{(abs.)}$ is calculated as 0.998.

The part of "$G \times Loss_{(system)}$" is calculated as

$$G \times Loss_{(system)} = 10^{20/10} \times 10^{-20.5/10} = 0.933 \qquad (2.24).$$

The pulse number $m_{(CO2)}$ is

$$m_{(CO2)} = \log_{0.998}^{0.933} = 56 \qquad (2.25).$$

Based on this estimation, 56 pulses are needed for 4% CO_2 sensing with a 10 m length sensing waveguide.

2.4 Conclusions

In this chapter we first introduced the principle of infrared absorption spectroscopy and CRDS. Based on these two gas sensing principles, we proposed waveguide CRDS for hand-held size breath sensor. Because waveguide propagation loss prevents ppm-order gas sensing, the amplifier-assisted scheme is proposed. In order to verify the effectiveness of the amplifier-assisted waveguide CRDS, an EDFA is used in the experimental set-up for compensating the waveguide propagation loss. As a result, with EDFA gain of 5 dB, the looping time (pulse number) increased to 16 from only a few. These results lead to the sensing path length extending more than 5 times than that without amplification.

Moreover, the pulse number is related to the cavity ring-down time. The gas concentration is estimated by the cavity ring-down time. In this chapter,

the necessary pulse number estimation for ppm-order gas concentration is given in this chapter. For instance, 56 pulses are needed for 4% CO_2 measurement with a 10 m length silica high-mesa waveguide at EDFA gain of 20 dB.

References

[1] A. Barth, “Infrared spectroscopy of proteins”, Biochim. et Biophys. Acta-Bioenerg., **1767**(9), 1073-1101 (2007).

[2] Y. Ozaki, and H. Maeda, “Nondestructive analysis by near-infrared spectroscopy”, J. of Jpn. Society of Infrared Sci. and Tech., **5**(2), 78-88, (1995).

[3] T. Shimosaka, “Highly sensitive method for trace gas analysis”, Bunseiki Kagaku, **57**(9), 715-740 2008.

[4] D. F. Swinehart, “The beer-lambert law”, J. of Chem. Educ., **39**(7), 333-335 (1962).

[5] M. Kawasaki, and S. Enami, “Detection of trace species with cavity ring-down spectroscopy”, Laser Rev., **34**(4), 289-294 (2006).

[6] P. D. Bievre, and H. S. Peiser, “Atomic weight’: The name, its history, definition, and units”, Pure and Appl. Chem., **64**(10), 1535-1543 (1992).

[7] A. Laugier, and J. Garai, “Derivation of the ideal gas law”, J. of Chem. Educ., **84**(11), 1832-1833 (2007).

[8] Z. Q. Liu, and R. L. Wang, “Gas detection with infrared absorption principle”, Coal Sci. and Tech., **1**, 21-23 (2005).

[9] D. Roccarina, E. C. Lauritano, M. Gabrielli, F. Franceschi, V. Ojetti, and A. Gasbarrini, “The role of methane in intestinal disease”, The Am. J. of gastroenterol., **105**(6), 1250-1256 (2010).

[10] H. Zan, W. Tsai, Y. Lo, Y. Wu, and Y. Yang, “Pentacene-based organic thin film transistors for ammonia sensing”, IEEE Sens. J., **12**(3), 594-601 (2011).

[11] K. Kao, M. Hsu, Y. Chang, S. Gwo, and J. Andrew Yeh, “A sub-ppm acetone gas sensor for diabetes detection using 10nm thick ultrathin InN FETs”, Sens., **12**(6), 7157-7168 (2012).

[12] C. Turner, C. Walton, S. Hoashi, and M, Evans, “Breath acetone concentration decreases with blood glucose concentration in type 1 diabetes mellitus patients during hypoglycaemic clamps”, J. of Breath Res., **3**(4), 046004 (2009).

[13] P. Paredi, W. Biernacki, G. Invernizzi, S. A. Kharitnov, and P. J. Barnes, “Exhaled carbon monoxide levels elevated in diabetes and correlated with glucose concentration in blood: a new test for monitoring the disease?”, Chest, **116**(4), 1007-1011 (1999).

[14] K. Iitani, K. Toma, T. Arakawa, and K. Mitsubayashi, “Transcutaneous blood VOC imaging system (Skin-Gas Cam) with real-time bio-fluorometric device on rounded skin surface”, ACS Sens., **5**(2), 338-345 (2019).

[15] M. Kawasaki, and S. Enami, “Detection of trace species with cavity ring-down spectroscopy”, The Rev. of Laser Eng., **34**(4), 289-294 (2006).

[16] K. Tonokura, S. Marui, and M. Koshi, “Absorption cross-section measurements of the vinyl radical in the 440-460 nm region by cavity ring-down spectroscopy” Chem. Phys. Lett., **313**, 771-776 (1999).

[17] M. C. Chan, and S. H. Yeung, “High-resolution cavity enhanced absorption spectroscopy using phase-sensitive detection”, Chem. Phys. Lett., **373**(1-2), 100-108 (2003).

[18] J. J. Scherer, D. Voelkel, D. J. Rakestraw, “Infrared cavity ringdown laser absorption spectroscopy (IR-CRLAS) in low pressure flames”, Appl. Phys. B: Lasers and Opt., **64**(6), 1535-1543 (1992).

[19] H. Hokazono, W. Y. Li, S. Enami, H. S. Jiang, and K. Hamamoto, “Gas sensing demonstration by using silica high-mesa waveguide with amplified cavity ring down spectroscopy technique”, IEICE Electron. Express, **12** (15), 20150574 (2015).

[20] S. S. Brown, “Absorption spectroscopy in high-finesses cavities for atmospheric studies,” Chem. Rev., **103**(12), 5219-5238 (2003).

[21] M. Mazurenka, A. J. Orr-Ewing, R. Peverall and G. A. D. Ritchie “4 Cavity ring-down and cavity enhanced spectroscopy using diode lasers”, Annu. Rep. Prog. Chem., Sect. C: Phys. chem., **101**, 100-142 (2005).

[22] A. O'Keefe, and D. AG. Deacon, “Cavity ring-down optical spectrometer for absorption measurements using pulsed laser sources”, Rev. of Sci. Instr., **59**(12), 2544-2551 (1988).

[23] P. Zalicki, and R. N. Zare, “Cavity ring-down spectroscopy for quantitative absorption measurements” The J. of Chem. Phys., **102**(7), 2708-2717 (1995).

[24] Y. Ninomiya, M. Goto, S. Hashimoto, Y. Kagawa, K. Yoshizawa, M. Kawasaki, T. J. Wallington, and M. D.Hurley “Cavity ring-down spectroscopy and relative rate study of reactions of HCO radicals with O_2, NO, NO_2, and Cl_2 at 295 K” J. Phys. Chem. A. **104**, 7556-7564 (2000).

[25] S. Wolff, A. R. Giehl, M. Rennoo, and H. Fouckhardt, “Metallic waveguide mirrors in polymer film waveguides”, Appl. Phys. B, **73**, 623-627 (2001).

[26] B. S. Kawasaki, K. O. Hill, and R. G. Lamont, “Biconical-tapper single-mode fiber coupler”, Opt. Lett., **6**(7), 327-328 (1981).

Chapter 3

Issues and solutions in amplifier-assisted CRDS

3.1 Introductory overview

In waveguide CRDS, gas absorption happens when sensing light propagating in the waveguide. One problem is that waveguide has propagation loss. The propagation loss decreases the sensing light intensity. The rest part of sensing light intensity is not sufficient for ppm-order gas sensing. To compensate the waveguide propagation loss, we have proposed amplifier-assisted waveguide CRDS [1]. For realizing the hand-held gas sensor, the SOA (semiconductor optical amplifier) is a candidate. This is because SOA is capable for integrating. In order to evaluate the performance of the amplifier-assisted waveguide CRDS, we used an EDFA (Erbium-doped fiber amplifier) in the experimental system to compensate the propagation loss.

In amplifier-assisted waveguide CRDS sensing result (light intensity as a function of time); theoretically; the pulse number should increase with the EDFA gain increasing. In the experimental result; however; the pulse number was not changing with EDFA gain increasing at all. This is because self-lasing issue happens in the amplifier-assisted CRDS. When self-lasing happens, most of the EDFA gain is consumed at the self-lasing wavelength.

Sensing light is not amplified sufficiently. Moreover, amplifier noise is an unavoidable issue in amplifier-assisted CRDS. The amplifier noise [2] exists at the same wavelength with the sensing light. High amplifier noise prevents ppm-order gas sensing. This is because the necessary sensing light pulse may be covered behind the amplifier noise in the sensing result.

In this chapter, we first introduced the loss and the necessary gain in amplifier-assisted CRDS. Then we show the phenomenon of the self-lasing issue and amplifier noise issue. Next, we discuss about the reasons of these two issues and provide the solutions of these two issues. Finally, we show the results after solving the issues. Section 3.2 shows the gain and necessary gain in amplifier-assisted CRDS. Section 3.3 and 3.4 are the reason discussion and the solution for self-lasing issue, respectively. From section 3.5 and 3.6 are the reason discussion and the solutions for amplifier noise issue. The conclusion of this chapter is summarized in section 3.7.

3.2 Loss and gain in amplifier-assisted waveguide CRDS

In the amplifier-assisted CRDS experimental system, an EDFA is used inside a closed loop. EDFA provides gain to amplify the sensing light intensity. Figure 3.1 shows the experimental system of the amplifier-assisted waveguide CRDS.

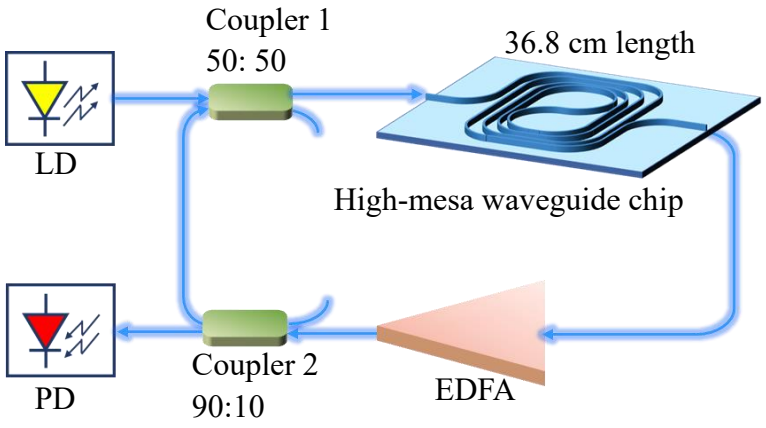

Fig. 3.1 Experimental system of amplifier-assisted waveguide CRDS. The loss of this system is coming from the waveguide and two couplers.

The sensing light coming out from the waveguide is guided to EDFA for amplification. Then, the amplified sensing light is guided back to the waveguide for gas absorption via optical coupler. The reason of why optical coupler being used in the system is because optical coupler realizes a portion of "leak-out" light goes out of the system for monitoring. As shown in Fig. 3.1, the amplified sensing light is guided back to waveguide via coupler 2 (90:10 coupler in this experiment). Coupler 2 also allows 10% leak-out light goes to PD (photo detector) for light intensity monitoring. Meanwhile, most of the sensing light (90%) is guided back to waveguide for gas absorption. Coupler 1 introduces the sensing pulse into the waveguide both from LD (Laser diode) and coupler 2. We chose the splitting ratio of coupler 1 as 50: 50 in this experiment. This is because 50:50 coupler makes a balance between the injection light intensity from LD and the "guided back light"

intensity from coupler 2. Neither these two parts of light intensity has a large intensity reduction by coupler 1.

The loss in this system is mainly coming from the waveguide and two couplers. In the experimental system, the loss of coupler 1 and coupler 2 are -3 dB and -0.5 dB, respectively. The high-mesa waveguide is 36.8 cm length. The waveguide is coupling with fiber in order to connect into the sensing system. The insertion loss of the waveguide is -7 dB (measured in 21st May 2012 in experiment). The -7 dB insertion loss includes -0.74 dB propagation loss (-0.02 dB/cm × 36.8 cm) and -6.26 dB coupling loss (-3.13 dB/facet).

The waveguide insertion loss; however; is measured as -21.2 dB in experiment recently (22nd March 2020). The loss increasing is because water vapor in air attached to the waveguide. The attached water vapor increases the waveguide absorption loss. The way to reduce the absorption loss is heating the waveguide to vaporize the water vapor. In order to prevent the water vapor attaching to the waveguide again, the heating should be down in flowing Nitrogen (N_2) environment.

In this experiment, we count the waveguide insertion loss as -21.2 dB. The total loss in the experimental system is -24.7 dB.

The necessary gain value is based on the loss in waveguide CRDS system. In this experiment, the necessary gain should be ≥ 24.7 dB. The gain of

EDFA as a function of pumping current in EDFA is shown in Fig. 3.2.

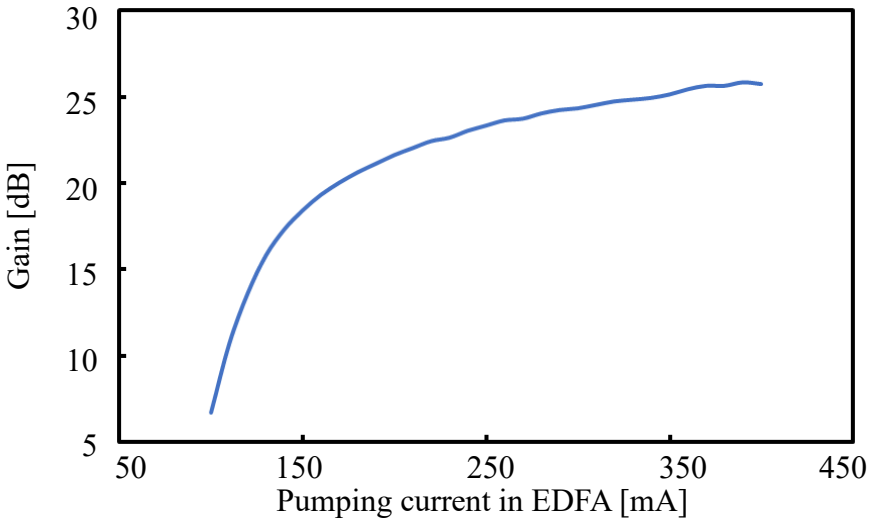

Fig. 3.2 EDFA gain at different pumping current in EDFA (@ 1572 nm). When the pumping current in EDFA is 400 mA, EDFA gain reaches 25.7 dB.

As shown in this figure, when pumping current in EDFA is 300 mA, the gain is 24.3 dB. When the pumping current in EDFA is 400 mA, the gain reaches to 25.7 dB. Therefore, the pumping current in EDFA is required to be more than 350 mA in this experiment.

Figure 3.3 shows the EDFA gain as a function of input light intensity. As shown in this figure, when input light intensity is between -40 dBm and -22 dBm, EDFA provides a stable gain around 23 dB. This is the static gain. When light intensity changes 1 dB, the dynamic gain only changes 0.1 dB. In the sensing system, pulses with different light intensity (light intensity difference less than 1 dB) are injecting into the EDFA. The dynamic gain of 0.1 dB changing is stable enough in this experimental system.

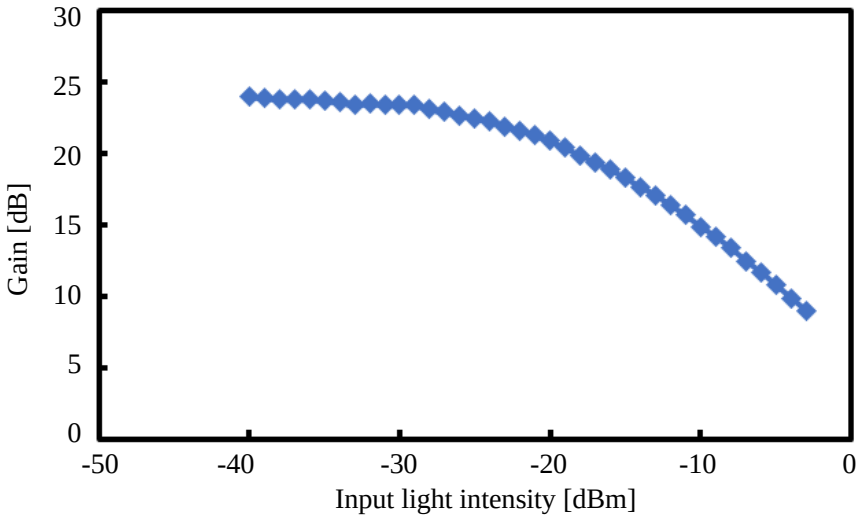

Fig. 3.3 EDFA gain as a function of input light intensity (pumping current = 250 mA). When input light intensity is between -40 dBm and -22 dBm, EDFA provides a stable gain around 23 dB. When light intensity changes 1 dB, the gain changes 0.1 dB.

3.3 Self-lasing issue

By calculating the loss in the amplifier-assisted waveguide CRDS, we know that the total loss in the system is -24.7 dB. The pumping current in EDFA should be ≥ 350 mA to ensure the gain ≥ 24.7 dB. In the experimental system, as EDFA gain increasing; theoretically; the sensing light should have high light intensity. The pulse number should increase.

The sensing experiment results (light intensity as a function of time); however; is different from the theoretical results. The sensing results under different EDFA gain are shown in Fig. 3.4.

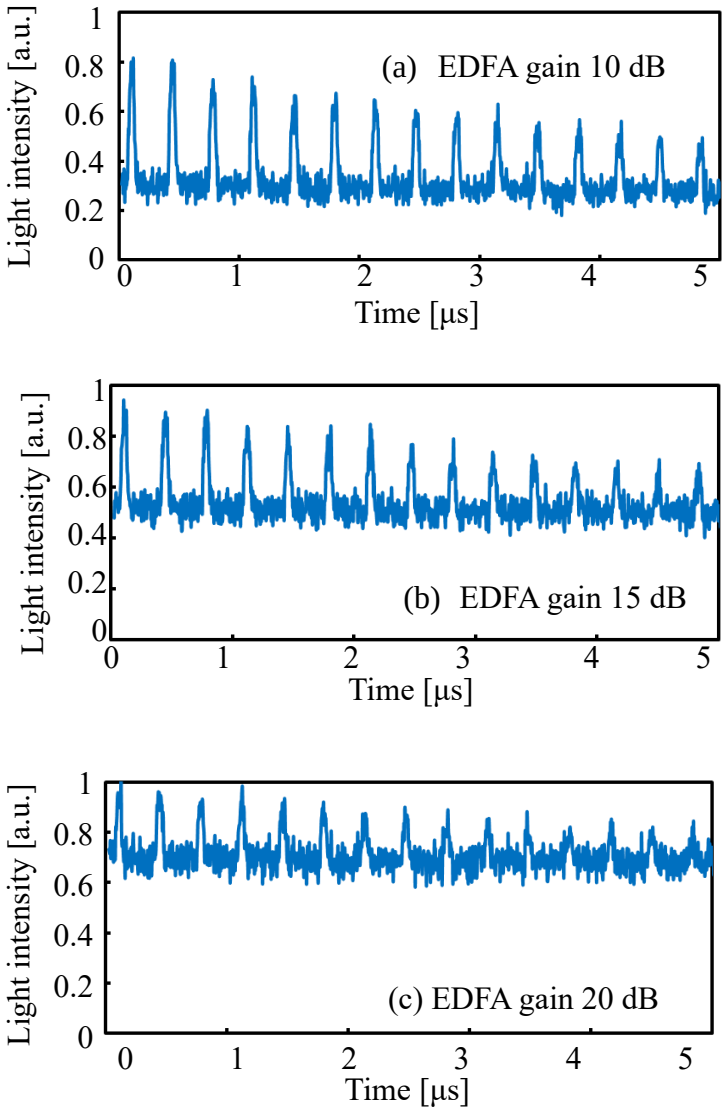

Fig. 3.4 Sensing results (light intensity as a function of time) under different EDFA gain. The background level of the pulse-train raised up with EDFA gain increasing, while pulse number had no change.

As shown in this figure, when EDFA gain increased from 10 dB to 20 dB, the pulse number in the pulse-train; however; had no change at all. The background level of the pulse-train raised a lot. This is because EDFA in CRDS (a closed loop) results in self-lasing issue when EDFA is at high pumping condition [3]. Figure 3.5 shows the optical spectrum of the

amplifier-assisted CRDS under different pumping current of EDFA. Sensing light wavelength was at 1572 nm, which is CO_2 absorption wavelength.

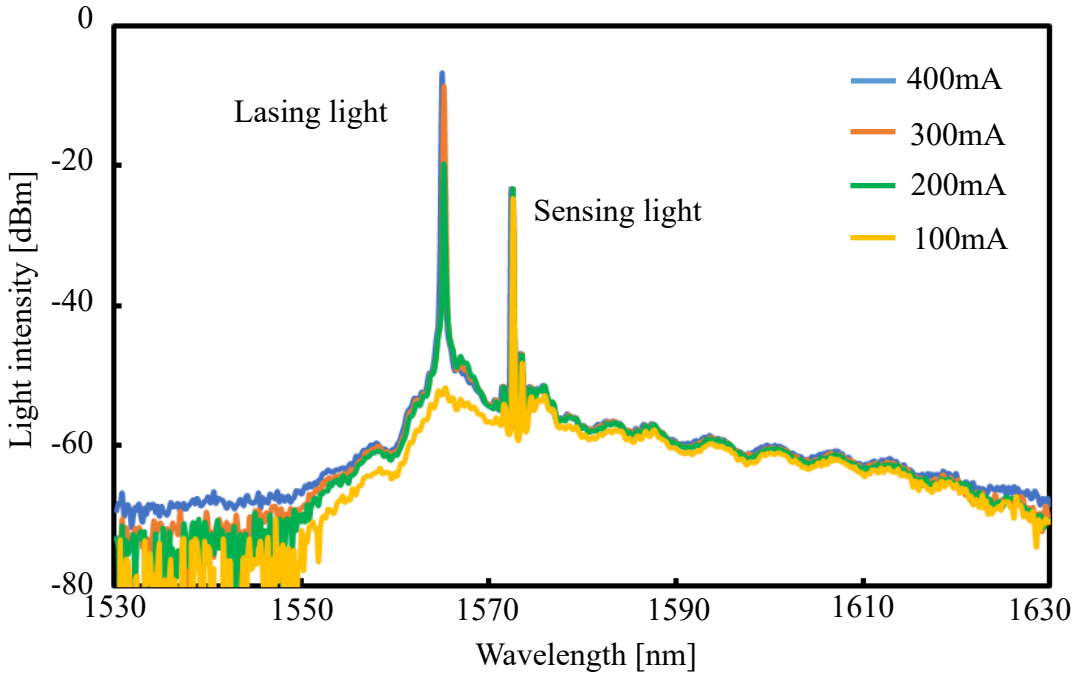

Fig. 3.5 Spectrum of amplifier-assisted CRDS under different pumping current in the EDFA. Self-lasing happened at 1564 nm wavelength. As the pumping current in the EDFA increasing, self-lasing light intensity increased to -7 dBm, while the sensing light intensity kept at -24 dBm.

As shown in the figure, self-lasing happened at 1564 nm wavelength. It seems that the self-lasing happened when injection current of the pumping LD in the EDFA was increased from 100 mA. As is indicated, the light intensity at self-lasing wavelength increased from -53 dBm to -7 dBm whereas the intensity at sensing light wavelength kept at -24 dBm. Figure 3.6 shows the gains at self-lasing wavelength and sensing light wavelength. As shown in this figure, when pumping current in EDFA increasing, the gain

at self-lasing wavelength is increasing. While the gain at sensing light wavelength is kept at 14 dB. Therefore, Once this self-lasing happens, sensing light is not amplified sufficiently because most of the amplifier gain is attributed to the lasing wavelength. Therefore, in the sensing result, the pulse number had no change at all. The background increasing is because of the self-lasing light intensity increasing.

We think the reason of self-lasing happening at 1564 nm is because EDFA gain dependents on wavelength [4]. In EDFA gain spectrum, wavelength between 1530 nm-1560 nm gets higher gain, compared to 1570 nm wavelength. 1564 nm lasing light getting gain easier than 1572 nm wavelength, so most of the gain is consumed at the self-lasing wavelength.

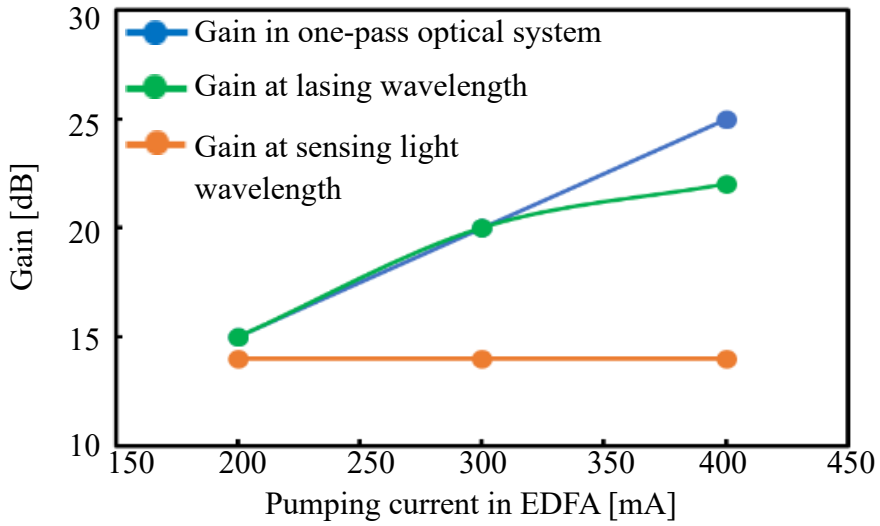

Fig. 3.6 The gains that EDFA provided to the sensing light and to the self-lasing light. When self-lasing happens, most of the gain is consumed by self-lasing wavelength. The gain at sensing light wavelength is fixed at 14 dB.

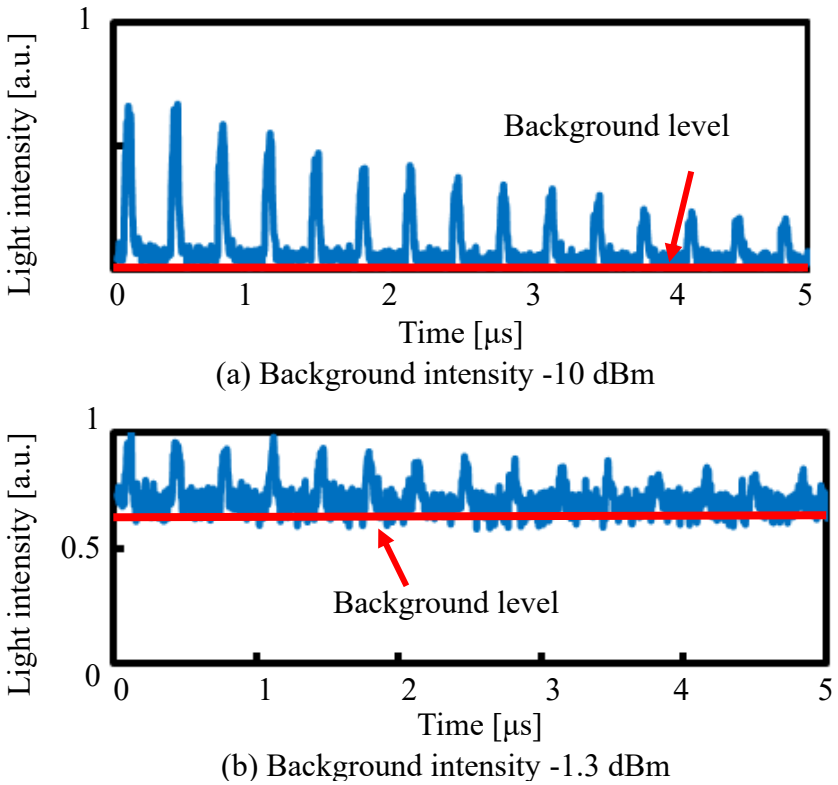

Fig. 3.7 Sensing results under different pumping current in EDFA of (a) 50 mA, and (b) 300 mA. The background level increased from -10 dBm to -1.3 dBm because of the self-lasing.

As mentioned above, the reason of pulse-train background level raising is because of self-lasing. In Fig. 3.7 we compared the sensing results under pumping current in EDFA of (a) 50 mA and (b) 300 mA. At the condition of EDFA pumping current of 300 mA, the self-lasing light get much gain rather than the case of 50 mA. As a result, the background level raised from light intensity 0 [a.u.] (-10 dBm) to 0.7 [a.u.] (-1.3 dBm). From the time of 4 μs, the pulses are surpassed by the background level. This pulse-train is not available for gas concentration measurement.

Figure 3.8 shows a brief schematic of self-lasing happening. In amplifier-

assisted CRDS system, lasing happens when coherency [5] is secured, which means that the traveling light wave has the same frequency, polarization, and phase [6]. The "first seed" of the self-lasing is the ASE (amplified spontaneous emission) of EDFA [4]. When the Er^{3+} is pumped to produce a population inversion in EDFA, ASE is generated due to the spontaneous emission. The "first seed" ASE travels inside the amplifier-assisted CRDS. The ASE loops back to the EDFA which keeps "coherency" and be amplified. When the travelling ASE intensity reaches lasing threshold, self-lasing happens.

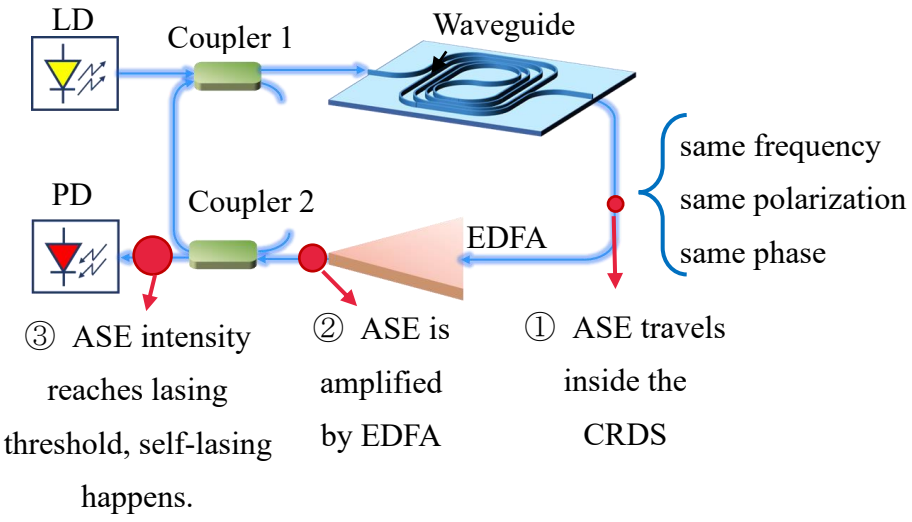

Fig. 3.8 The schematic of self-lasing in amplifier-assisted CRDS. ASE that is generated by EDFA travels inside the CRDS and be amplified by EDFA. When the ASE intensity reaches lasing threshold, self-lasing happens.

3.4 Self-lasing issue solution: polarization direction control scheme

To suspend the self-lasing, we proposed polarization direction control scheme. This method is with changing the polarization direction of the travelling light wave to weaken the coherency condition. Figure 3.9 shows the experimental system of the polarization direction control scheme.

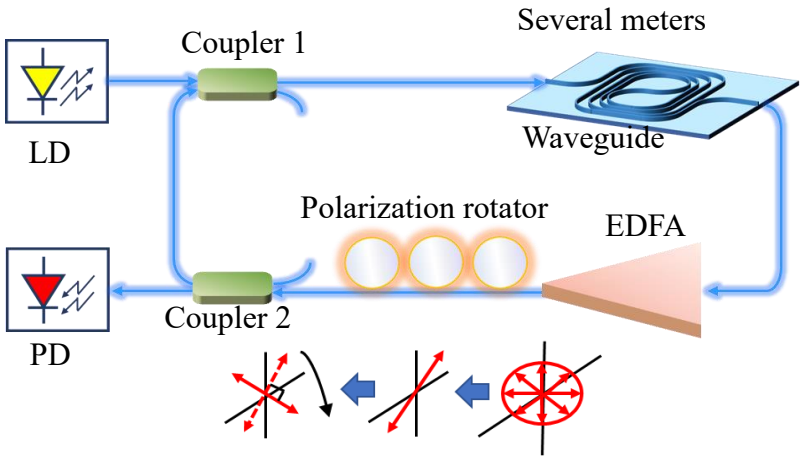

Fig. 3.9 Polarization direction control scheme for suspending self-lasing. A polarization rotator is added in the amplifier-assisted CRDS. The non-linear polarization light is firstly turned to linear polarization light. Then the polarization direction of the linear polarization light is rotated 90° to weaken the coherency condition. Then, self-lasing is stopped.

A 3-stage polarization rotator with a polarizer, a 1/4 wave plate and a 1/2 wave plate is set into the cycle loop after EDFA. The ASE coming out from EDFA is non-linear polarization light [7]. The polarizer is used to alter the ASE polarization state to linear polarization. The direction of the linear polarization light is changed by rotating the 1/2 wave plate. The 90°rotation

of the polarization direction mostly weaken the coherency condition. Hence, self-lasing is suspended.

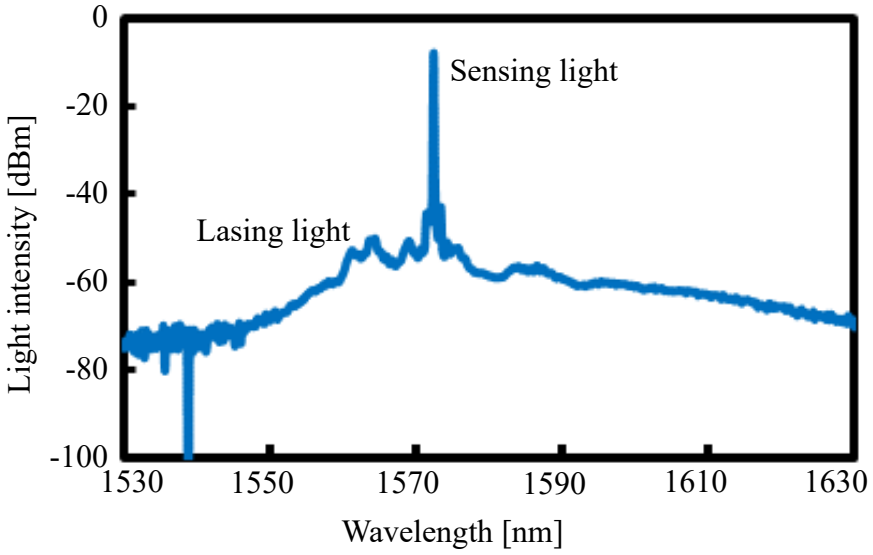

Fig. 3.10 Spectrum of the polarization direction control scheme. The lasing light intensity is suspended down below -50 dBm. The gain at sensing light wavelength is estimated as 24 dB.

The result of the polarization direction control scheme is confirmed by using the optical spectrum from the output port of coupler 2. The result is shown in Fig. 3.10. As shown in this spectrum, the self-lasing intensity was suspended below -50 dBm. We estimated that the gain at sensing light wavelength increased to 24 dB from 14 dB.

This is the case of amplifier-assisted CRDS using EDFA to compensate the loss. In our future work, SOA is used as the amplifier on the gas sensing chip. ASE that generated by SOA is linear polarization light [8]. By integrating polarization rotating device onto the chip, the result of self-lasing

suspending should be achieved as the case of EDFA.

3.5 Amplifier noise issue

Whereas self-lasing issue was solved, the amplifier noise is a serious problem in the amplifier-assisted CRDS. The amplifier noise exists at a wide wavelength band ranging from 1530 nm to 1630 nm, including the sensing light wavelength. The amplifier noise is hardly eliminated. The noise intensity is accumulating while the amplifier noise looping inside the CRDS. In ppm-order gas sensing, after more than 1,000 times looping, the accumulated amplifier noise intensity may exceed the sensing light intensity. The intensity of the accumulated amplifier noise; therefore; directly influences the sensing ability of the amplifier-assisted CRDS.

The amplifier noise is mainly caused by the spontaneous emission in EDFA [9] and the amplified signal light. Figure 3.11 shows the energy level scheme of ground, and the first two excited states of erbium ions in a silica matrix [10].

In this figure, level 1 represents the ground state. Level 2 represents metastable state, and level 3 represents excited state. Erbium ions are excited to higher energy state from ground state by pumping light. Different pumping light wavelength excites the erbium ions to different energy level.

980nm wavelength pumping light excites erbium ions to level 3, and 1480nm wavelength pumping light excites erbium ions to level 2. Erbium ions at level 3 is not stable. The lifetime of the Er at level 3 is 1~10μs [6, 11]. Erbium ions at level 3 is back to level 2 very soon. The phenomenon that Erbium ions at level 2 emits photons and returns back to ground level without signal injection is spontaneous emission. The spontaneous emission is a main reason of amplifier noise.

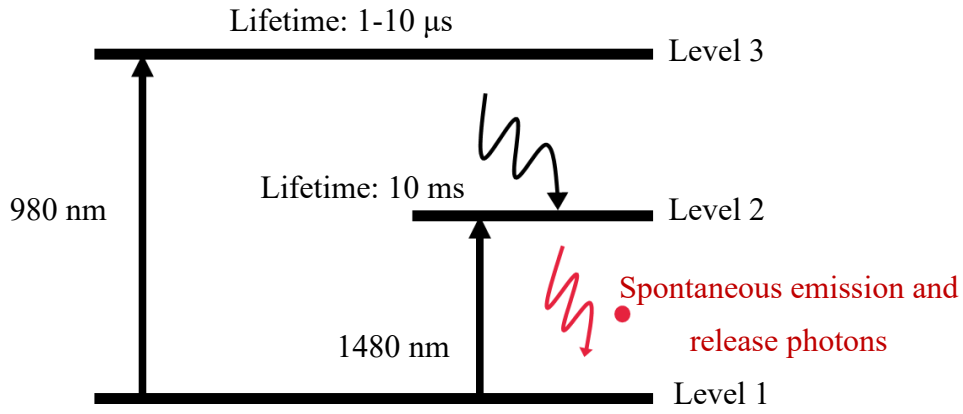

Fig. 3.11 Energy level scheme of ground, and the first two excited states of Erbium ions in a silica matrix. Spontaneous emission causes the amplifier noise.

Another reason that causes amplifier noise is the signal light. When signal light injects into EDFA, it introduces shot noise [12] into the system. Moreover, in the EDFA, different frequency of two optical carriers causes beat noise [13]. As a summary, the amplifier noise mainly comes from four parts [4]: (a) Shot noise caused by amplified signal light; (b) Shot noise caused by spontaneous emission light; (c) Beat noise between signal light

and spontaneous emission light; and (d) Beat noise between spontaneous emission light. Among these four kinds of amplifier noises, noises (a) and (c) are at the same wavelength with the sensing light. Noises (b) and (d) are at different wavelength from the sensing light. These two noises are eliminated easily by using a wavelength filter. Wavelength filter in the breath sensing system; however; limits several kind of gases sensing. Therefore, the amplifier noise is unavoidable.

Figure 3.12 (a) shows the spectrum of amplifier-assisted CRDS under different gain of EDFA with sensing light injection. In this spectrum, as the gain of EDFA raising from 5 dB to 20 dB, not only the light intensity of signal light increased, the light intensity level of the other wavelength also increased about 30 dB. The increasing light intensity level at the other wavelength is because of the noise (b) and (d). Figure 3.9 (b) are the spectrum under different gain of EDFA with no sensing light injection. In this spectrum, at the sensing light wavelength of 1572 nm, the light intensity increased 20 dB while the gain of EDFA raising from 5 dB to 20 dB. This is because of the amplifier noise (a) and (c).

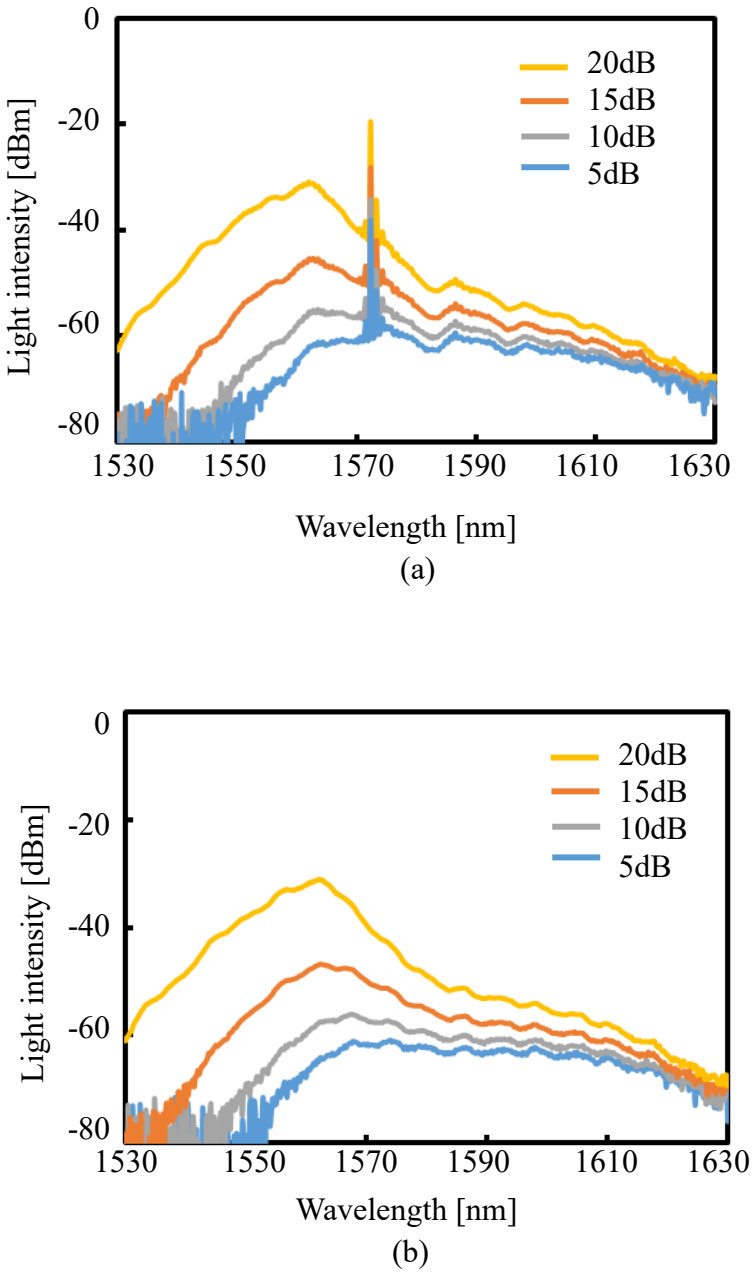

Fig. 3.12 Spectrum of amplifier-assisted CRDS under different gain of EDFA with (a) 1572 nm sensing light, and (b) no sensing light. The increasing light intensity at the other wavelength is because of amplifier noise (b) and (d). In spectrum (b), the increasing light intensity at 1572 nm wavelength is because of amplifier noise (a) and (c).

3.6 Amplifier noise issue solution

3.6.1 Additional loss control

To suppress the amplifier noise intensity, we proposed the scheme of additional loss control, by using the excess loss to suppress the amplifier noise intensity. As shown in Fig. 3.13, a power-attenuator is introduced into the amplifier-assisted CRDS to provide the actual excess loss.

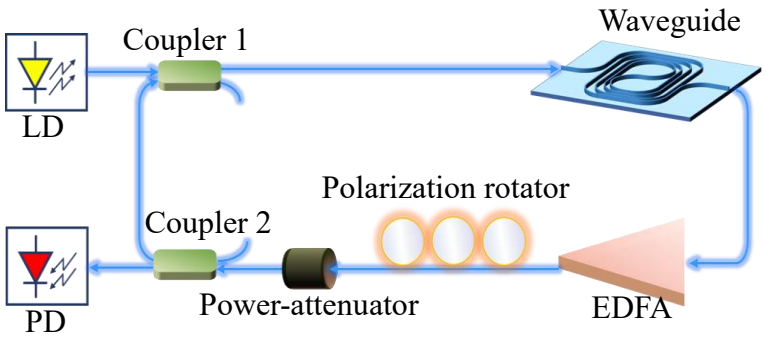

Fig. 3.13 Additional loss scheme for suppressing amplifier noise. A power-attenuator is set inside amplifier-assisted CRDS for providing extra loss.

Figure 3.14 is the optical spectrum of amplifier-assisted CRDS at different loss of the power-attenuator. At the loss of power-attenuator is 15 dB, the ASE power is suppressed down below -50 dBm, also the signal power is suppressed.

The amplifier noise intensity is decreased by the additional loss. The noise level in the sensing result (light intensity as a function of time) is suppressed. This leads to a higher extinction ratio of pulse. The pulses that were hidden by the amplifier noise show up. Much more pulses are achieved

in the pulse-train.

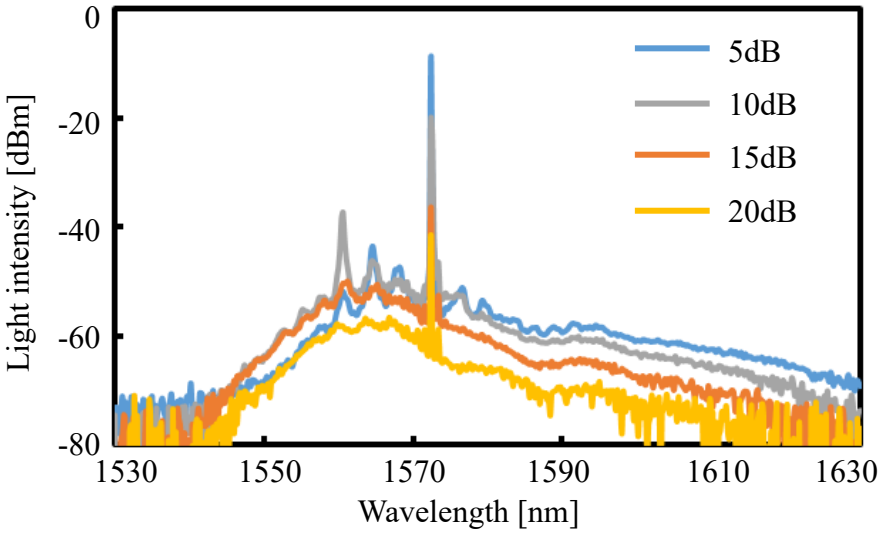

Fig. 3.14 Spectrum of amplifier-assisted CRDS under different loss of power-attenuator. The light intensity at self-lasing wavelength was suppressed down below -50 dBm when power-attenuator provided 15 dB loss.

The sensing result after polarization direction control and additional loss control is shown in Fig. 3.15. The background noise level is suppressed to an extremely low level. Although the sensing light intensity is also suppressed, the power-attenuator decreased the amplifier noise intensity and kept the high gain level of EDFA simultaneously. Sensing light is amplified sufficiently. As shown in Fig. 3.15, more than 200 pulses have been achieved. This result corresponds to the ability for 10 ppm-order CH_4 (intestinal disease marker) detection.

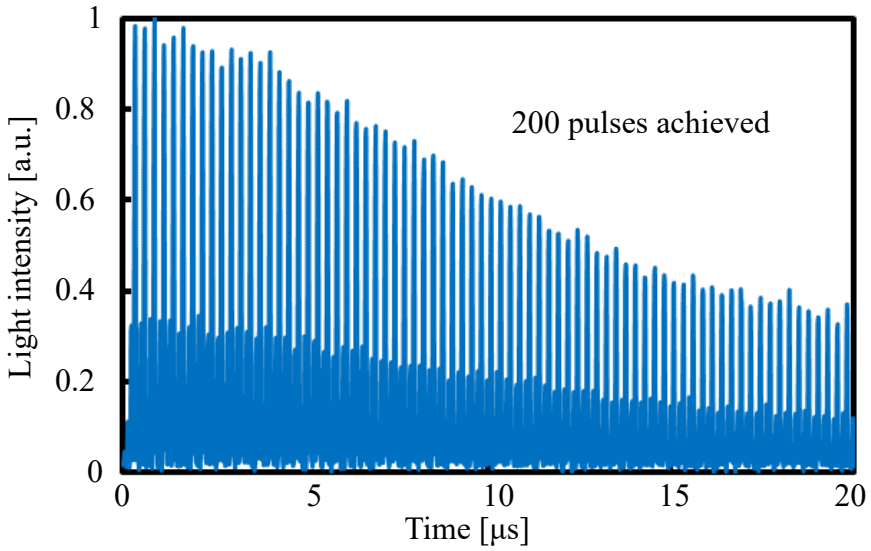

Fig. 3.15 Sensing result with polarization direction control and additional loss control. Sensing light was amplified sufficiently because self-lasing was suspended. 200 pulses are achieved in the pulse-train.

Additional loss control is proved effective for suppressing amplifier noise intensity. This result indicates a higher tolerance of the waveguide propagation loss. A relatively large waveguide propagation loss allows longer sensing path. Meanwhile, the waveguide propagation loss suppresses the amplifier noise intensity.

3.6.2 Sufficient injection light intensity control

To a certain extent, additional loss control decreases the amplifier noise intensity. Because the sensing light intensity is also be suppressed by the additional loss, the way to decrease amplifier noise intensity by using extra loss has limitation. In ppm-order gas sensing, the accumulated amplifier

noise is as large as -3 dBm. Suppressing this large noise and ensuring the sensing light get enough gain impossibly realize at the same time. The sensing still suffers the influence of the amplifier noise in ppm-order gas sensing. To realize ppm-order sensing by using amplifier-assisted CRDS, after n times looping, the sensing light intensity I_s [dBm] is required to be larger than the accumulated noise intensity I_n. To compare the intensity of I_n and I_s, we need to calculate the amplifier noise intensity and the sensing light intensity.

The intensity of the amplifier noise is calculated by the amplifier noise figure (*NF*) [4, 6].

$$NF = \left(\frac{Signal}{Noise}\right)_{IN} / \left(\frac{Signal}{Noise}\right)_{OUT} \tag{3.1}$$

When we change the *NF* into log-scale in [dB], eq. (3) becomes as follows:

$$NF = [(Signal)_{IN} - (Signal)_{OUT}] - [(Noise)_{IN} - (Noise)_{OUT}] \tag{3.2}$$

The gain G [dB] is expressed by $(Signal)_{OUT}$ and $(Signal)_{IN}$ as:

$$G = (Signal)_{OUT} - (Signal)_{IN} \tag{3.3}$$

$(Noise)_{IN}$ [dBm] is the input thermal noise, which is expressed as:

$$(Noise)_{IN} = 10 \times \log_{10}(kTB \times 10^3) \tag{3.4}$$

Here, k is Boltzmann constant, T [K] is temperature, and B [Hz] is the bandwidth. Then the amplifier noise intensity $(Noise)_{OUT}$ is written as:

$$(Noise)_{OUT} = NF + G + 10 \times \log_{10}(kTB \times 10^3) \tag{3.5}$$

In this case, we take *NF* as 3 dB in the calculation, because in EDFA the

quantum limit of *NF* is 3 dB when the population inversion occurs sufficiently [14]. Based on the co-doped materials of Erbium-doped fiber [4, 15, 16], EDFA has a stable gain that ranges from 15 dB to 40 dB. So, we assume that the gain is stable at 20 dB in this calculation. At the condition of T = 298 K (25 °C) and sensing wavelength λ = 1572 nm, $(Noise)_{OUT}$ is calculated as -43 dBm (i.e., 50 nW). Then the accumulated noise intensity I_n [dBm]is calculated as:

$$I_n = 10\times\log_{10}(n\times 50\times 10^{-6}) \tag{3.6}$$

where n is the times that the noise looping inside the system.

In 4% CO_2 (major gas in exhaled breath) sensing for instance, the necessary looping time is 56 (calculated in Section 2.3). With n = 56, the accumulated noise intensity is calculated as -25.5 dBm.

The sensing light intensity after n times loop I_s is calculated as:

$$I_s = 10\times\log_{10}\{I_0\times[\exp(-\sigma NL\times\frac{P\times NA\times 10^{-9}}{RT}\times\Gamma_{air})]^{n}\} \tag{3.7}$$

I_0 [mW]is the injection light intensity. l [cm] is the waveguide length and Γ_{out} [%] is the portion of light profiles that comes out of the waveguide for gas absorption. The term of "exp $(-\sigma NL\times\frac{P\times NA\times 10^{-9}}{RT}\times\Gamma_{air})$" donates to the gas absorption attenuation in one loop. The value of I_s is available to be enhanced by increasing the injection light intensity I_0.

We used 4 gases (acetone, methane, ammonia, and carbon dioxide), to

confirm the sensing ability of amplifier-assisted CRDS. We calculated the amplifier noise intensity I_n and the necessary injection light intensity I_0 for each gas. In this calculation, the system loss and the amplifier gain were all set as 20 dB (ideal condition). The light intensity criteria was 1/e. The calculated results are shown in Fig. 3. 16.

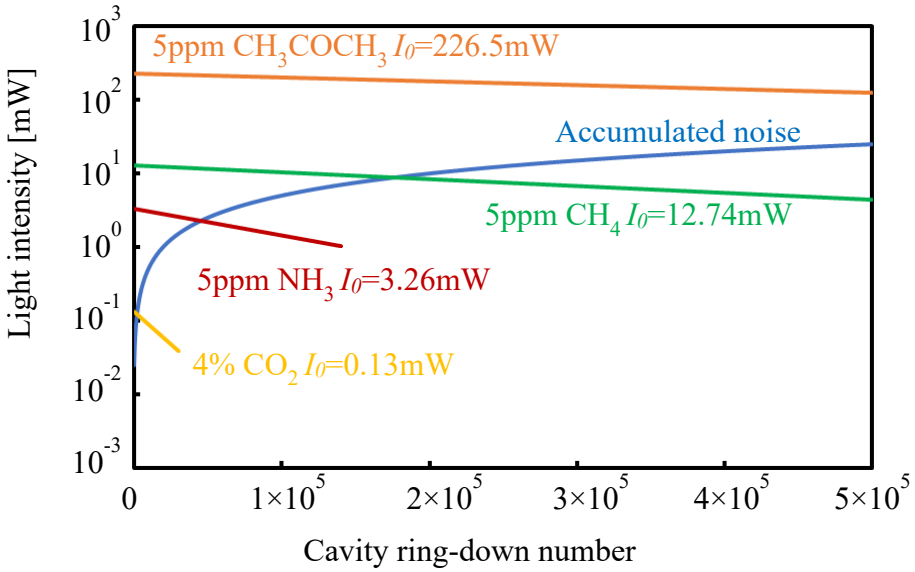

Fig. 3.16 Calculated accumulated amplifier noise and the necessary injection light intensity for different gases. The methane, ammonia, and carbon dioxide in exhaled breath are detectable with I_0 below 13 mW. While acetone sensing requires I_0 as large as 226.5 mW.

In this figure, it shows the accumulated noise intensity I_n and the sensing light intensity as a function of the cavity ring-down number. The blue line shows the accumulated noise intensity I_n. The orange, green, red, and yellow line show the sensing light intensity decreasing tendency for acetone, methane, ammonia, and carbon dioxide, respectively. Based on the estimation above, the concentration of CO_2 in human breath (40,000 ppm) is

detectable with 0.13 mW injection light intensity. The methane, and ammonia in exhaled breath are detectable with injection light below 13 mW. While acetone sensing requires the injection light as large as 226.5 mW.

Most of the EDFA provides a stable gain when input light intensity is in between -40 dBm~ -20 dBm [4, 6, 17]. The injection light intensity I_0 has an intensity limitation to ensure the stable gain of amplifier. The light intensity range of I_0 is estimated as: 0 dBm (1mW) $\leq I_0 \leq$ 10 dBm (10 mW), considering the loss of the waveguide (the loss is estimated as -20 dB). Therefore, 226.5 mW injection light for acetone sensing is hard to realize. One way to decrease the I0 is to increase the light intensity criteria. Figure 3.17 shows the calculated results of amplifier noise and injection light when the light intensity criteria is 0.9.

When the light intensity increased from 1/e (i.e. 0.37) to 0.9, the cavity ring-down number decreased. The accumulated amplifier noise intensity decreased with the decreased cavity ring-down number. Thus, the necessary injection light intensity is decreased. With the light intensity criteria of 0.9, 5ppm acetone is detectable within 10 mW.

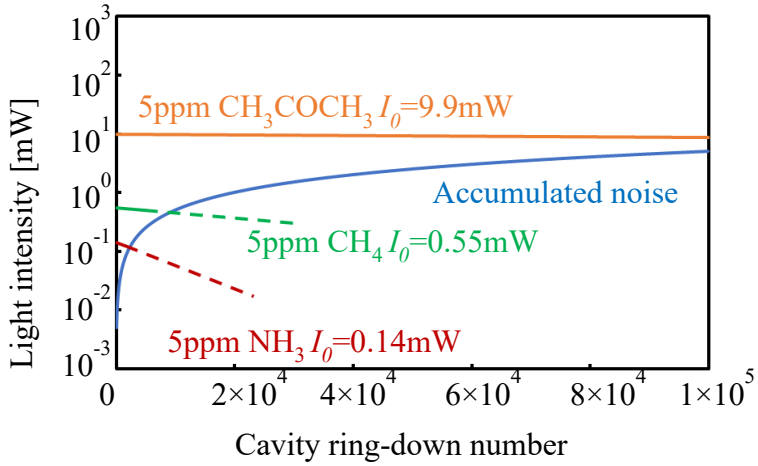

Fig. 3.17 Calculated accumulated amplifier noise and the necessary injection light intensity for different gases when light intensity criteria was 0.9. The 5ppm acetone are detectable within 10 mW injection light intensity because of the increased criteria.

According to the analysis above, ppm-order gas concentration is detectable with the influence of amplifier noise. Amplifier-assisted CRDS is available for ppm-order gas sensing, as long as we control the injection light intensity.

3.7 Conclusions

In amplifier-assisted CRDS, self-lasing issue happens when EDFA is at high pumping condition. Self-lasing light consumes most of the EDFA gain. Sensing light is not amplified sufficiently. To suspend the self-lasing, we proposed the polarization direction control. The “coherency” condition is weakened by changing the polarization direction of the travelling ASE. Thus, self-lasing is stopped. As a result, the self-lasing light intensity was

suspended down below -50 dBm from -7 dBm. The gain at sensing light wavelength increased to 24 dB from 14 dB.

Whereas the self-lasing issue is solved, there is an important issue in amplifier-assisted CRDS. The amplifier noise is hardly eliminated. The amplifier noise loops inside the sensing system. The noise intensity is accumulating. The large accumulated amplifier noise may cover the necessary sensing pulses for ppm-order gas sensing. Thus, ppm-order gas sensing is impossible with the accumulated amplifier noise. To suppress the amplifier noise intensity, we proposed additional loss scheme. By using the extra loss in the amplifier-assisted CRDS, the amplifier noise intensity was suppressed down below -50 dBm. In the sensing result (light intensity as a function of time), more than 200 pulses have been achieved. This result is available for 10 ppm-order CH_4 (intestinal disease marker) detection. The additional loss control scheme indicates a higher tolerance of waveguide propagation loss.

The additional loss control has limitation in suppressing amplifier noise intensity. This is because sensing light intensity is also decreased by the extra loss. In order to sensing ppm-order gas under the influence of amplifier noise, one requirement is to use sufficient light intensity. One requirement of the injection light intensity I_0 is that 0 dBm (1mW) $\leq I_0 \leq$ 10 dBm (10 mW). This is because the amplifier provides a stable gain when light intensity is in this

range. Based on the calculation, the concentration of CO_2 in human breath (40,000 ppm) is detectable with 0.13 mW injection light intensity when the light intensity criteria is set as 1/e (i.e. 0.37). By increasing the light intensity criteria, the necessary sensing light intensity decreases. When the light intensity criteria is set as 0.9, the methane, ammonia, and acetone in exhaled breath are all detectable within 10 mW injection light intensity.

Reference

[1] M. Tsujino, H. Hokazono, J. Chen, and K. Hamamoto, “Optical amplifier assisted cavity ring down spectroscopy (CRDS) method for compact infrared sensing”, Tech. Dig. MOC, **H57**, 1-2 (2013).

[2] B. Min, H. Yoon, W. J. Lee, and N. Park, “Coupled structure for wide-band EDFA with gain and noise figure improvements from C to L-band ASE injection”, IEEE Photonics Tech. Lett. **12**(5), 480-482 (2000).

[3] J. Chow, G. Town, B. Eggleton, M. Ibsen, K. Sugden, and I. Bennion, “Multiwavelength generation in an erbium- doped fiber laser using in-fiber comb filters”, IEEE Photonics Tech. Lett., **8**(1), 60-62 (1996).

[4] M. Nakazawa, *Erbium doped fiber amplifier*, Optronics, Tokyo (1999) Chap. 1 [in Japanese].

[5] L. Mandel, and E. Wolf, *Optical coherency and quantum optics*, Cambridge university press, UK (1995) Chap. 4.

[6] Ter-Mikirtychev, and Vartan, *Fundamentals of fiber lasers and fiber amplifiers*, Springer, Swizerland (2014) Chap. 7.

[7] M. G. Taylor, “Observation of new polarization dependence effect in long haul optically amplified system”, IEEE Photonics Tech. Lett., **5**(10), 1244-1246 (1993).

[8] G. Contestabile, L. Banchi, M. Presi, and E. Ciaramella, “Investigation of transparency of FWM in SOA to advanced modulation formats

involving intensity, phase, and polarization multiplexing", J. of Lightwave Tech., **27**(19), 4256-4261 (2009).

[9] A.C. Cokrak, and A. Altuncu, "Gain and noise figure performance of erbium doped fiber amplifiers (EDFA)", Istanbul University J. of Electrical & Electronics Engineering, **4**(2), 1111-1122 (2004).

[10] R. I. Laming, S. B. Poole, and E. J. Tarbox, "Pump excited-state absorption in erbium-doped fibers", Opt. Lett., **13**(12), 1084-1086 (1988).

[11] L. Chiaraviglio, P. Wiatr, P. Monti, J. Chen, L. Wosinska, J. Lorincz, F. Idzikowski, and M. Listanti, "Impact of energy-efficient techniques on a device lifetime", IEEE Online Conference on Green Communications, 1-6 (2014).

[12] K. J. Williams, and R. D. Esman, "Optically amplified downconverting link with shot-noise-limited performance", IEEE Photonics Tech. Lett., **8**(1), 148-150 (1996).

[13] W. H. Powell, and M. S. Waddington, "SCM based passive optical network with noise monitoring and control", The Proc. 13th Annual Conference on European Fiber Optic Communications and Networks, **1**, 138-139 (1995).

[14] E. Desurvire, D. Bayart, B. Desthieux, and S. Bigo. *Erbium-doped fiber amplifiers: device and system developments*, Wiley- Interscience, New York (2002) Chap. 5.

[15] S. Tanaka, K. Imai, T. Yazaki, H. Tanaka, T. Yamashita, and M. Yoshida, "Ultra-wideband L-band EDFA using phosphorus co-doped silica-fiber", Opt. Fiber Communications Conference, P. ThJ3 (2002).

[16] H. Masuda, and Y. Miyamoto, "Low-noise extended L-band phosphorus co-doped silicate EDFA consisting of novel two-stage gain-flattened gain blocks", Electronics Lett., 44(18), 1082-1083 (2008).

Chapter 4

CO_2 gas sensing experiments

4.1 Introductory overview

We have proposed polarization direction control to suspend the self-lasing issue. Based on the estimation in section 3.5.2, more than 10 ppm CO_2 are sensing available by using injection light intensity of 1 mW. In this chapter, we use CO_2 as the sample gas to do the actual sensing experiment.

In section 4.2, the first demonstration of CO_2 sensing with amplifier-assisted waveguide CRDS is introduced.

In section 4.3, the result of 3% CO_2 sensing by using injection light intensity of 1 mW is introduced.

The conclusions are summarized in section 4.4.

4.2 First demonstration of CO_2 sensing with amplifier-assisted waveguide CRDS

In order to prove whether the amplifier-assisted waveguide CRDS is available for real gas sensing, we first used high concentration (10^5 order) CO_2 to check the sensing ability of the amplifier-assisted waveguide CRDS. The experimental set-up is shown in Fig. 4.1.

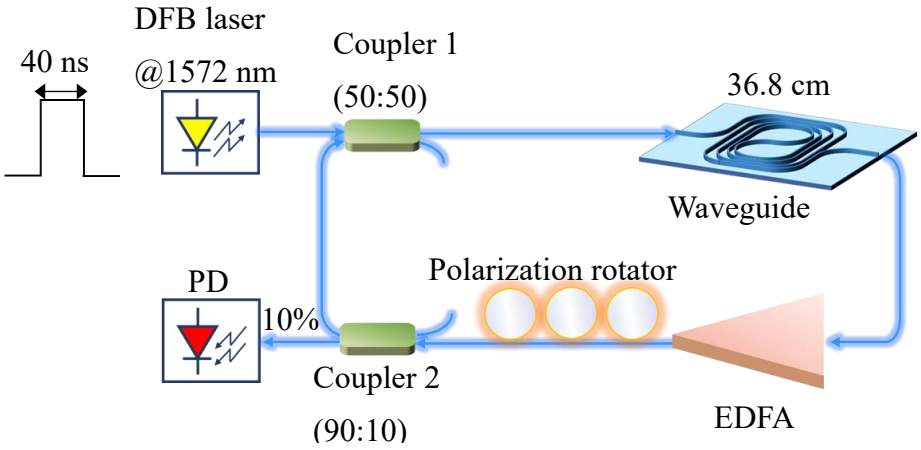

Fig. 4.1 Experimental set-up for CO_2 sensing. A 36.8 cm length silica high-mesa waveguide was used. The Sensing pulse light was at 1572 nm wavelength, which is CO_2 absorption wavelength. The pulse width is 40 ns.

A DFB laser (Anritsu, mode: AB6A234P2) was used as the light source. Its center wavelength is 1572nm, which is the absorption wavelength of CO_2. The DFB laser was controlled by a pulse pattern generator (Agilent 81130A) to generate the sensing pulse. The sensing pulse intensity was 1 mW. The pulse width was set as 40 ns. Period was set as 18 μs. This means one pulse is injected into the CRDS system by every 18 μs.

The reason of using pulse period of 18 μs is because this pulse period realizes gain clumping. Fig. 4.2 shows the sensing result (light intensity as a function of time) with pulse period of (a) 35 μs, and (b) 18 μs. In Fig. 4.2 (a), the cavity ring-down time [1] (The time that light intensity decreases to the criteria (normally 1/e)) was around 20 μs. In the time range of 20 μs ~ 35 μs, the sensing light intensity was low. When the second pulse injected into EDFA, self-lasing happened in EDFA. By decreasing the pumping current in

EDFA down below lasing threshold, the self-lasing was terminated. We got the decreasing waveform as shown in Fig.4.2 (a). The pulse-train was not decreasing stably. This is because the gain of EDFA is unstable.

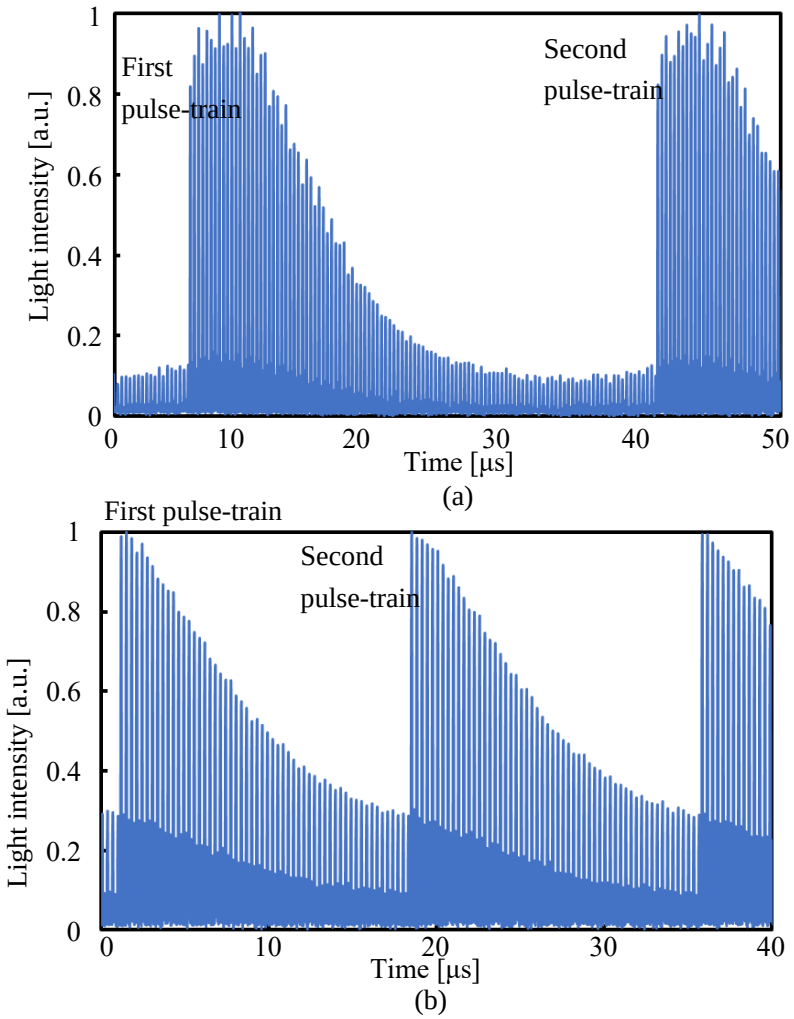

Fig. 4.2 Sensing result (light intensity as a function of time) with pulse period of (a) 35 μs, and (b) 18 μs. Large pulse period resulted in self-lasing in EDFA. The unstable gain caused pulse light intensity fluctuation. By shortening the pulse period, the second pulse-train was introduced into the system before the cavity ring-down time. The gain is clumped. Therefore, the pulse intensity increased. The pulse-train became smooth.

In order to achieve stable gain, the pulse period was shortened. The

second pulse-train was introduced into the sensing system before the cavity ring-down time. The gain was clumped. The gain became stable. As shown in Fig. 4.2 (b), the pulse period was 18 μs, which is shorter than the cavity ring-down time (20 μs). Due to the gain clumping, the pulse intensity decreased smoothly.

In the experimental system, coupler 2 is used to guide the amplified sensing light back to waveguide. Coupler 1 is used to introduce both injected light and the amplified light into the waveguide. Both coupler 1 and coupler 2 are polarization maintaining fiber coupler. In this experiment, the splitting ratio of coupler 1 (Thorlabs, PMC1550-50B-APC) was 50: 50. Every time the light propagating through coupler 1, the light intensity decreased 3 dB. The reason of using 50:50 coupler is because the injection light intensity only decreases 3 dB comparing to 90:10 coupler (decrease 10 dB) or 99: 1 coupler (decrease 20 dB). The 3 dB loss that sensing light return back to the CRDS is compensated by EDFA. The splitting ratio of coupler 2 (Thorlabs, PMC1550-90B-APC-1) was 90:10. The 10% output port was connected to the oscilloscope for monitoring. The light intensity that goes to oscilloscope via coupler 2 decreased 10 dB. The 10 dB decreased sensing light intensity is in the detectable range of oscilloscope. The 90% output port of coupler 2 was connected to coupler 1. It is used to guide most of the sensing light back into the waveguide. The light intensity guided back to coupler 1 decreased

0.46 dB.

The polarization rotator for self-lasing suspending was a 3-stage polarization rotator from Optoquest Co., LTD. It is consist of a polarizer, a quarter waveplate, and a half wave plate.

EDFA (AMP-FL8002-LB) was a commercial product from FiberLabs. It provides gain at both C and L band. The EDFA was operated at the ACC (auto current control) mode. In the ACC mode the gain is kept constant [2]. The performance of the EDFA at 1572 nm wavelength were mentioned in Fig. 3.2 and Fig. 3.3 in Chap. 3. The EDFA provides a gain of 26 dB when pumping current in EDFA is 400 mA. When input light intensity is in the range of -40 dBm ~ -22 dBm, EDFA gain has a 3 dB decrease. When input light intensity is in this range, EDFA provides a stable gain around 23 dB. The dynamic gain has 0.1 dB changing when input light has 1 dB changing. Therefore, when the input light intensity is in the range of -40 dBm ~ -22 dBm, EDFA provides a stable gain.

In this experiment, the sensing waveguide was 36.8 cm length. The waveguide chip had been coupled with fibers for the sensing experiment. The outside view of the waveguide chip and the coupling fibers are shown in Fig. 4.3.

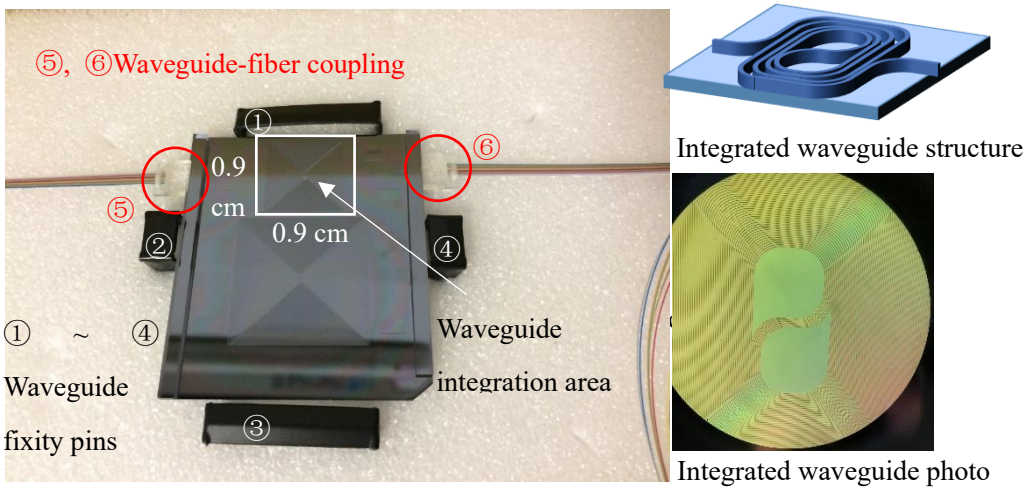

Fig. 4.3 Output view of the silica high-mesa waveguide chip. The chip is coupled with optical fiber for the sensing experiment. Six 36.8 cm length waveguide are integrated in a 0.9 cm × 0.9 cm area.

On this chip, six 36.8 cm length waveguides are integrated on the chip in a 0.9 cm × 0.9 cm area. These six waveguides have different width. Due to the waveguide width difference, the performance of these six waveguides are different. The waveguide No., waveguide width, its insertion loss, and the Γ_{air} are summarized in Tab. 4.1.

From this table, No. 3 waveguide with waveguide width of 2.23 μm has a low insertion loss of 21.24 dB and a Γ_{air} of 3%. We chose this waveguide to be used in the sensing experiment.

Tab. 4.1 The insertion loss, and Γ_{air} of the waveguides at 4.5 cm length. The No. 3 waveguide has a lowest insertion loss of 21.24 dB, and a high Γ_{air} of 3%.

Waveguide No.	Waveguide length [cm]	Waveguide width [μm]	Γ_{air} [%]	Insertion loss [dB]
1	36.8	2.63	1.9	16.97
2	36.8	2.43	2.4	18.09
3	36.8	2.23	3	21.24
4	36.8	2.13	0.14	23.93
5	36.8	1.93	0.13	29.29
6	36.8	1.73		37.65

The waveguide is set into a vacuum gas chamber. The outside view of the gas chamber is shown in Fig. 4.4. The fibers in blue color at the left-hand side of the chamber connects the waveguide to the sensing system. CO_2 gas is inserted into the vacuum chamber from the right-hand side. The amount of the CO_2 is controlled by the pressure meter. Based on the Ideal gas law [3]:

$$PV=nRT \quad (1),$$

The volume V, and the temperature T are constants in this experiment. The amount of CO_2 n is proportional to the pressure in chamber P. In the case of getting sensing result without CO_2, the same amount of N_2 whose absorption wavelength is not at 1572 nm is inserted into the vacuum gas chamber to ensure the same experiment condition.

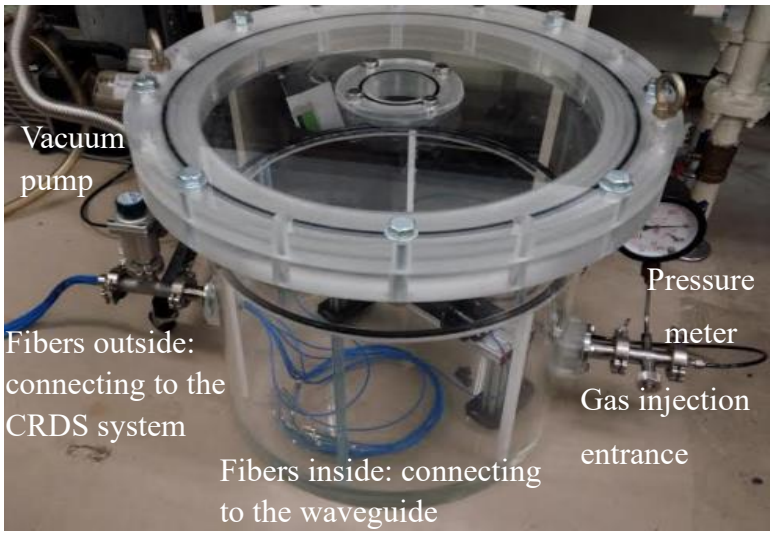

Fig. 4.4 The output view of the gas chamber. The fiber outside the chamber was used to connect the waveguide with the CRDS system. The fiber inside the chamber was used to connect the waveguide. The gas injection entrance is at the right-hand side. The pressure meter is used to control the concentration of the injected gas. The vacuum pump is used to vacuum the chamber.

In this experiment, we injected different concentration of CO_2 from 40% to 80% into the gas chamber. The sensing results are shown in Fig. 4.5.

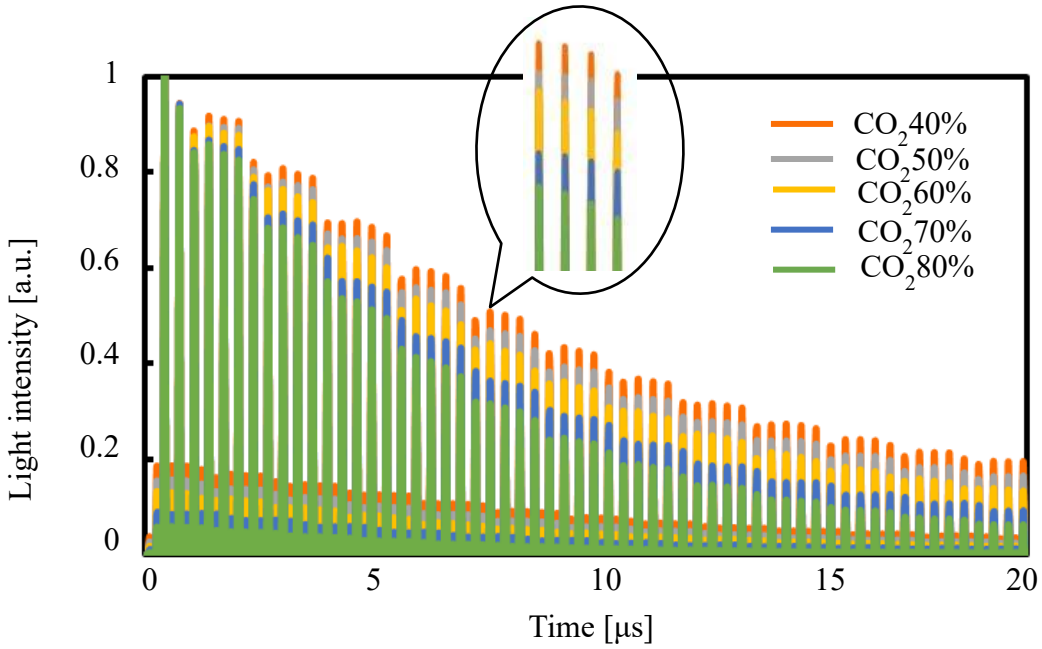

Fig. 4.5 CO_2 40%-80% sensing results. The light intensity decreased with the CO_2 concentration increasing due to the gas absorption.

As the CO_2 concentration increasing, the light intensity decreased as shown in this figure. This is because CO_2 absorbed more light intensity in higher concentration case. This sensing result proved that gas absorption really happened in the amplifier-assisted waveguide CRDS. The amplifier-assisted waveguide CRDS is capable for gas sensing.

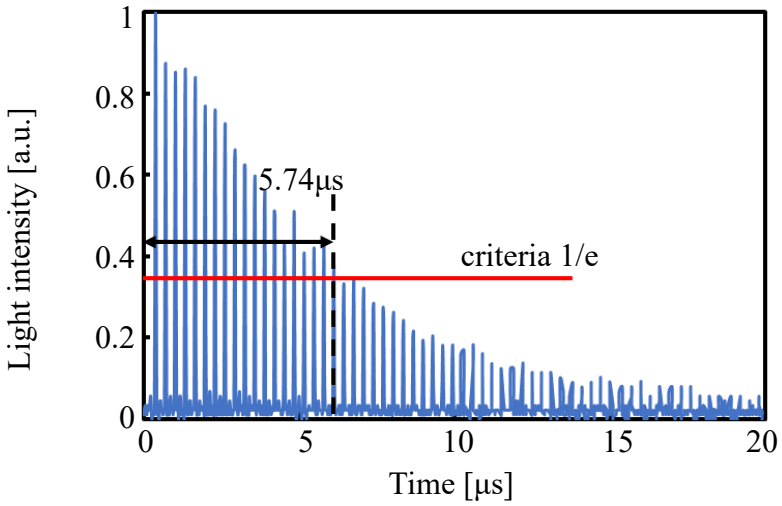

(a) With 40% CO_2

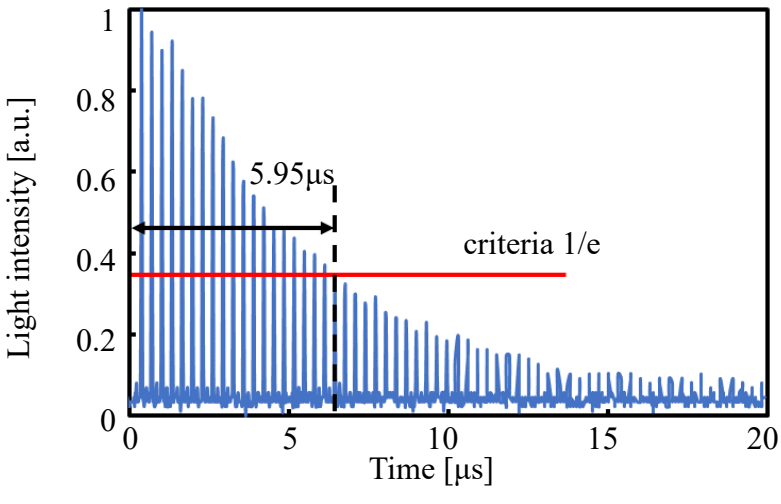

(b) Without CO_2

Fig. 4.6 Sensing results of (a) with 40% CO_2, and (b) without CO_2. The cavity ring-down time of (a) and (b) are 5.74μs and 5.95μs, respectively.

Next, we measured the CO_2 concentration by the sensing result. Figure 4.6 shows the 40% CO_2 sensing results. The red line is the criteria of 1/e for cavity ring-down time estimation. In the case of "with 40% CO_2", the cavity ring-down time is XX μs. In the case of "without CO_2", the cavity ring-down time is XX μs. The CO_2 concentration is estimated as XX%. This estimated result is very nearly to 40%.

The cavity ring-down times of the other CO_2 concentration and the estimated result are summarized in Tab. 4.2. As shown in this table, the sensing accuracy are all within 2% in all cases.

Tab. 4.2 The estimated CO_2 concentration and the cavity ring-down time. The sensing accuracy are all within 2%.

Absolute concentration of CO_2 [%]	Estimated result of CO_2 [%]	Cavity ring-down time [μs]	
		Without CO_2	With CO_2
70	70	11.38	9.47
60	58	10.05	8.93
50	51	16.46	14.28
40	39	5.95	5.75

4.3 3% CO_2 sensing result and analysis

Based on the calculation results in section 3.6.2, one requirement of the gas sensing under the influence of the amplifier noise is to use sufficient light intensity. For instance, the injection light intensity is required to be more

than 1 mW for CO_2. In this case, CO_2 concentration in human breath (40,000 ppm) is available for sensing. To confirm the actual availability, we tried 3% CO_2 gas sensing by using the amplifier-assisted CRDS with 1 mW injection light-pulse. In this experiment, the experimental set-up was the same as the one shown in Fig. 4.1. The light-pulse width was set as 10 ns. The period was set as 27 μs to reduce the ASE. With pulse period of 27 μs, the over-lap happened between the first and second pulse-train. The over-lap causes pulse light intensity fluctuation which leads to low sensing accuracy. We used pulse width of 10 ns instead of 40 ns is because we tried to avoid the pulse over-lap. Pulse with wide width over-laps with each other easily than that with narrow width.

The measurement results (light intensity as a function of time) are shown in Fig. 4.7. In this figure, (a) and (b) are the sensing results of "without CO_2" situation and "3% CO_2" situation, respectively. The orange line shows the light intensity decreasing trend. Because the pulse-train over-lap still happened, it is hard to estimate the cavity ring-down time with Fig. 4.7 (a), and (b). In order to analyze the light intensity of the pulse-train clearly, we took the light intensity data of each pulse peak. By using these data, we draw the approximate line. The pulse peak data intensity data and the approximate lines are shown in Fig. 4.8.

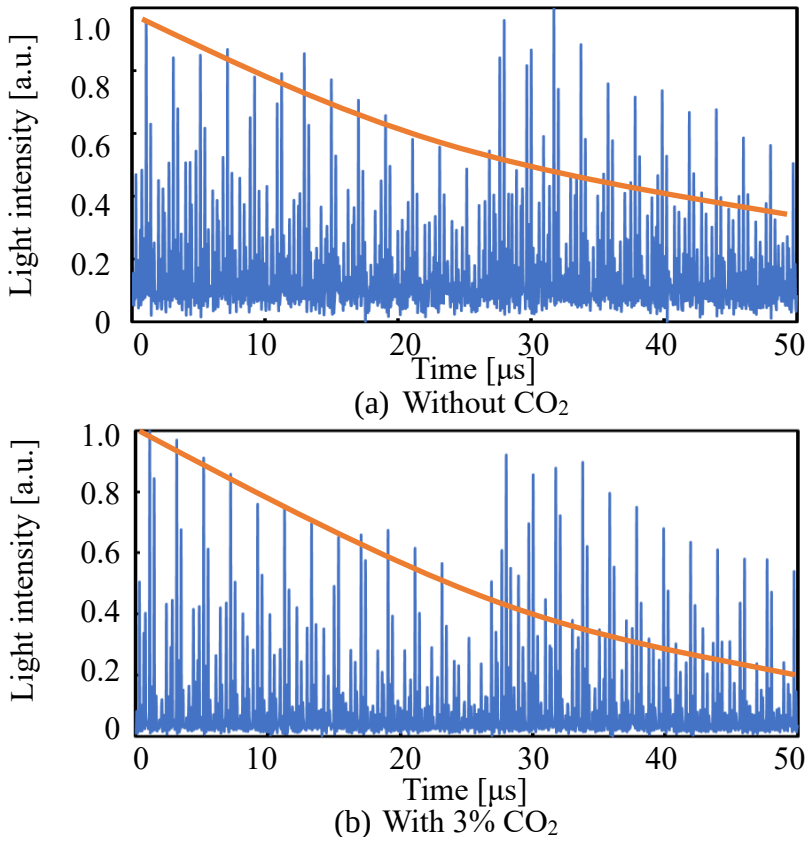

Fig. 4.7 Sensing result of (a) without CO_2, and (b) with 3% CO_2.

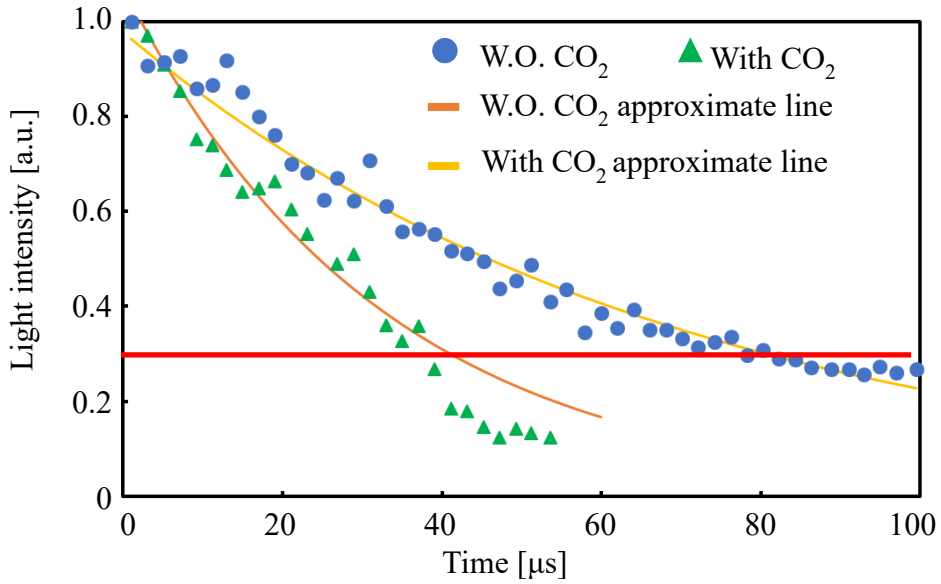

Fig. 4.8 Light intensity peak points and the approximate line of 3% CO2 sensing result. The cavity ring-down times are estimated as 41μs and 80.7 μs for "with" and "without" CO2 condition, respectively.

As shown in Fig. 4.8, the blue dots and green triangles are the light intensity data of "without CO_2" and "3% CO_2" situation, respectively. The orange line and the yellow line are the approximate lines. The cavity ring-down times for gas concentration measurement is defined by the light intensity criteria that we set. Here, the criteria level is near to the normal criteria level 1/e (red line in Fig. 4.8). The cavity ring-down times were estimated as 80.7 μs and 41 μs for "no CO_2" and "3% CO_2" situation, respectively. Because human breath contains 4% CO_2, in this work, the result of 3% CO_2 sensing indicates that the proposed amplifier-assisted CRDS enable breath sensing.

The estimated CO_2 concentration corresponds to be 1%, and the value was not exactly same with the injected gas condition. This difference may be because of the error in the accuracy of CO_2 density. As we mentioned above, the injected gas concentration is controlled by the pressure of the gas chamber. Figure 4.9 shows the pressure meter we used in the experiment. The meter dial accuracy was 0.002 Mpa. By using this pressure meter, the 3% CO_2 that injected into the gas chamber has an error of ±2%. Because the injected CO_2 was not proper 3%, the sensing error happened.

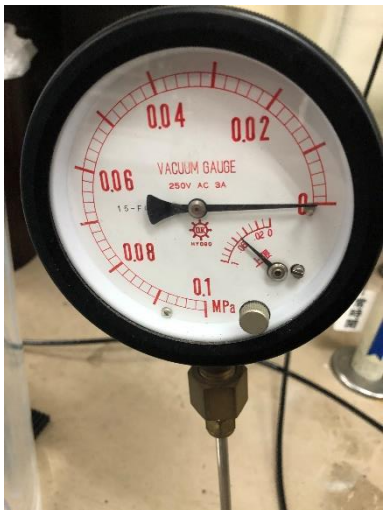

Fig. 4.9 The output view of the pressure meter. The meter dial accuracy was 0.002 Mpa. By using this pressure meter, the 3% CO_2 that injected into the gas chamber has an error of ±2%.

4.4 Conclusions

In this chapter, we reported the real CO_2 sensing by using amplifier-assisted waveguide CRDS. A 36.8 cm length silica high-mesa waveguide is used in the 80%-40% CO_2 sensing. The sensing result showed that CO_2 absorption happened. As the CO_2 concentration increasing from 40% to 80%, the light intensity decreased fast because of the gas absorption. This sensing result proved that amplifier-assisted CRDS is capable for gas sensing. Moreover, the CO_2 concentration estimation results showed that the sensing accuracy are within 2% in all cases.

We have proposed in section 3.6.2 that gas sensing is available under the influence of the amplifier noise. The requirement is the sufficient injection light intensity. To improve this proposal, we measured 3% CO_2 with a 36.8

cm length silica high-mesa waveguide by using 1 mW injection light intensity. As a result, 3% CO_2 was sensing successfully with cavity ring-down time of 41 μs and 80.7 μs for "without CO_2" and "with 3% CO_2" situation, respectively. The estimated concentration value of 1% was not exactly the same with the injected gas condition. This may because the gas injection control has an error of ±2%. The injected CO_2 concentration may be no proper 3%, so that the sensing error happened.

Reference

[1] H. Hokazono, W. Y. Li, S. Enami, H. S. Jiang, and K. Hamamoto, “Gas sensing demonstration by using silica high-mesa waveguide with amplified cavity ring down spectroscopy technique”, IEICE Electron. Express, **12** (15), 20150574 (2015).

[2] Finisa, “Introduction to EDFA technology”, Finisar White Pater, 1-6 (2009).

[3] A. Laugier, and J. Garai, “Derivation of the ideal gas law”, J. of Chem. Educ., **84**(11), 1832-1833 (2007).

Chapter 5

Conclusion and outlook

5.1 Conclusion

As mentioned in Chap. 1, home-based breath sensors are expected to present characteristics of hand-held size, high sensitivity and real-time sensing, and several gases sensing at the same time. Infrared absorption spectroscopy realizes several gases sensing at the same time. One problem is that ppm-order breath contents sensing by using infrared absorption needs a long sensing path as to km-order. In order to realize hand-held sensor, we proposed to use high-mesa waveguide as the sensing path. In this study, we discussed the gas sensing by using high-mesa waveguide.

In Chap. 2, the principle of gas sensing by using waveguide has been discussed. The waveguide CRDS system allows the sensing light propagation through the waveguide repeatedly. The corresponding sensing path length reaches km-order for ppm-order gas sensing. The problem is that waveguide propagation loss consumes most of the sensing light. The amplifier-assisted waveguide CRDS is proposed to compensate the propagation loss in this chapter.

In Chap. 3, we discussed about the issues in the proposed amplifier-

assisted waveguide CRDS. Amplifier in the closed CRDS loop; however; may result in self-lasing issue when amplifier is at high pumping condition. The self-lasing prevents the sensing light from being amplified sufficiently. We proposed polarization direction control scheme to suspend the self-lasing. As a result, the lasing light intensity was suppressed down below -50 dBm. The gain at sensing light wavelength increased to 24 dB from 14 dB. Besides the self-lasing issue, amplifier noise issue is a serious problem in amplifier-assisted CRDS. The amplifier noise is hardly eliminated. The accumulated noise intensity influences the sensing ability directly. We proposed additional loss control to suppress the amplifier noise intensity. As a result, the sensing light pulse with low light intensity showed up in the sensing result. 200 pulses are reached in the sensing result. This result is capable for 10 ppm-order methane sensing. One limitation of additional loss control is that the sensing light intensity is also suppressed. In order to sensing gas under the influence of the amplifier noise, one requirement is the sufficient injection light intensity. Based on the calculation, the concentration of CO_2 in human breath (40,000 ppm) is detectable with 0.13 mW injection light intensity when the light intensity criteria is set as 1/e (i.e. 0.37). By increasing the light intensity criteria, the necessary sensing light intensity decreases. When the light intensity criteria is set as 0.9, the methane, ammonia, and acetone in exhaled breath are all detectable within 10 mW injection light intensity.

In Chap. 4, we reported the CO2 sensing experiments and their results. The 70%- 40% CO2 sensing were successful within 17 μs. The sensing accuracy was within 2% in all case. We also successfully detected 3% CO_2 using 1 mW input sensing light intensity as a ring-down time difference (80 μs and 38 μs) based on the proposed amplifier-assisted CRDS. This result indicates that the amplifier-assisted CRDS is available for breath sensing.

5.2 Outlook

We have demonstrated that the amplifier-assisted waveguide CRDS is capable for breath sensing. To realize the amplifier-assisted waveguide CRDS on chip for hand-held sensor; however; some issues are not be discussed.

First is the light source. In order to sensing several gases, a light source that emits light at several wavelengths is expected. The SLED (super luminescent diode) emits light at a wide range of wavelength. It is a candidate of several gases sensing light source. If the SLED is used as the light source, a WDM (wavelength division multiplexing) is needed at the sensing system output part. The WDM is used to separate the light at gas absorption wavelength. Wavelength tunable laser is also a candidate of light source. By choosing the gas that we want to sense, the wavelength tunable laser emits the light at the absorption wavelength of the gas we choose.

Second is the amplifier. One candidate of on-chip amplifier is SOA. Based on our knowledge, SOA normally works in C-band. The light at wavelength larger than 1600 nm is hardly be amplified by SOA. The amplification for 1650 nm (methane absorption wavelength) and 1680 nm (acetone absorption wavelength) need to be discussed.

Third is the gas concentration estimation. A gas concentration estimation system needs to be set up. In this system, the optical signal from the sensing system is converted into electric signal by the photo detector. The electric signal is sent to the micro computer for sensing data analysis. Then the estimated gas concentration value is shown on the monitor.

Finally, we hope and believe that this amplifier-assisted waveguide CRDS will contribute to realize hand-held size breath sensor in future.

Appendix

A-1 Symbols used in this thesis

Symbols	Meaning
α	Propagation loss
Γ_{out}	Portion of light profiles that comes out of waveguide
N’	Density of the gas molecule
σ	Gas absorption cross-section
L	Interaction length between sensing light and the garget gas
I_{in}	Injection light intensity
I_{out}	Output light intensity
NA	Avogadro constant
n	Amount of the target gas
V_{total}	Total volume of the breath
V_{gas}	Volume of the target gas
N	Gas concentration
P	Pressure
T	Temperature
R	Ideal gas constant
λ	wavelength
τ_0	Decay life of the light in gas-cell
τ	Cavity ring-down time in the “no-gas in gas-cell” situation
τ_{gas}	Cavity ring-down time in the “gas in gas-cell” situation
t	Time
c	Light speed
G	Amplifier gain. indicates
$Loss_{(system)}$	Total loss in waveguide CRDS

$Loss_{(abs.)}$	Gas absorption loss
$Loss_{(waveguide)}$	Total waveguide loss
m	Required number of pulses at the situation of "no-gas",
$m_{(gas)}$	Required number of pulses at the situation of "with gas"
n	Sensing light looping times in waveguide CRDS
I_s	Sensing light intensity
I_n.	Accumulated noise intensity
$(Signal)_{IN}$	Input signal intensity
$(Signal)_{OUT}$	Output signal intensity
$(Noise)_{IN}$	Input thermal noise intensity
$(Noise)_{OUT}$	Output noise intensity
k	Boltzmann constant
B	Bandwidth
l	Waveguide length

A-2 Abbreviations used in this thesis

Abbreviations	Meaning
ECG	Electrocardiogram
VOCs	Volatile organic compounds
CRDS	Cavity ring-down spectroscopy
FOM	Figure of merits
SOA	Semiconductor optical amplifier
EDFA	Erbium-doped fiber amplifier
ASE	Amplified spontaneous emission
NF	Noise figure
ACC	Auto current control
SLED	Super luminescent Light-Emitting Diode
WDM	Wavelength-division-multiplexing

Acknowledgement

First of all, I would like to express my sincere gratitude and thanks to Professor Dr. Kiichi Hamamoto for his kind and cordial help to accomplish this research works in his laboratory. He taught me how to do research, how to think scientifically. His kind and valuable advices made me become a better man.

Secondly, I am expressing my sincere thanks to Assistant Professor Dr Haisong Jiang. She helped me a lot in my research and gave me many valuable advises in my study abroad life.

I would like to say thanks to all of my laboratory mates who helped me to do the experiments in the lab. I would like to give my special thanks to Dr Bingzhou Hong, Mr. Zanhui Chen, Ms. Yu Han, and Ms. Leiyun Wang for their valuable help in the laboratory during experiment.

I am also greatly indebted to the Professor Hiroshi Nakashima and Professor Kazutoshi Kato for reviewing my thesis carefully and their kind suggestions.

Last but not least, a cordial gratitude goes to my family and friends who is supporting me all these years during my study.